Discovery of novel thrips vector proteins that bind to the viral attachment protein of the plant bunyavirus, tomato spotted wilt virus

Ismael E. Badillo-Vargas[*a], Yuting Chen[*b], Kathleen M. Martin[b], Dorith Rotenberg[b#], and Anna E. Whitfield[b#]

[a]Department of Entomology, Texas A&M AgriLife Research, Weslaco, Texas, United States of America

[b]Department of Entomology and Plant Pathology, North Carolina State University, Raleigh, North Carolina, United States of America

Running head: Thrips proteins that interact with TSWV G_N

* IEBV and YC are joint first authors and contributed equally to this work.

Address correspondence to:

Anna E. Whitfield awhitfi@ncsu.edu and Dorith Rotenberg drotenb@ncsu.edu

Abstract

The plant-pathogenic virus, tomato spotted wilt virus (TSWV), encodes a structural glycoprotein (G_N) that, like with other bunyavirus/vector interactions, serves a role in viral attachment and possibly entry into arthropod vector host cells. It is well documented that *Frankliniella occidentalis* is one of seven competent thrips vectors of TSWV transmission to plant hosts, however, the insect molecules that interact with viral proteins, such as G_N, during infection and dissemination in thrips vector tissues are unknown. The goals of this project

were to identify TSWV-interacting proteins (TIPs) that interact directly with TSWV G_N and to localize expression of these proteins in relation to virus in thrips tissues of principle importance along the route of dissemination. We report here the identification of six TIPs from first instar larvae (L1), the most acquisition-efficient developmental stage of the thrips vector. Sequence analyses of these TIPs revealed homology to proteins associated with the infection cycle of other vector-borne viruses. Immunolocalization of the TIPs in L1s revealed robust expression in the midgut and salivary glands of *F. occidentalis*, the tissues most important during virus infection, replication and plant-inoculation. The TIPs and G_N interactions were validated using protein-protein interaction assays. Two of the thrips proteins, endocuticle structural glycoprotein and cyclophilin, were found to be consistent interactors with G_N. These newly discovered thrips protein-G_N interactions are essential towards better understanding of transmission of persistent propagative plant viruses by their vectors, as well as for developing new strategies of insect pest management and virus resistance in plants.

Importance Statement

Thrips-transmitted viruses cause devastating losses to numerous food crops worldwide. For negative-sense RNA viruses that infect plants, the arthropod serves as a host as well by supporting virus replication in specific tissues and organs of the vector. The goal of this work was to identify vector/host proteins that bind directly to the viral attachment protein and thus may play a role in the infection cycle in the insect. Using the model plant bunyavirus, tomato spotted wilt virus (TSWV), and the most efficient thrips vector, we identified and validated six TSWV-interacting proteins from *Frankliniella occidentalis* first instar larvae. Two proteins, an endocuticle structural glycoprotein and cyclophilin, were able to interact directly with the TSWV attachment protein, G_N, in insect cells. The TSWV G_N-interacting proteins

provide new targets for disrupting the virus-vector interaction and could be putative determinants of vector competence.

Introduction

Vector-borne diseases caused by animal- and plant-infecting viruses are some of the most important medical, veterinary, and agricultural problems worldwide (1, 2). The majority of viruses infecting plants and animals are transmitted by arthropods. Understanding the viral and arthropod determinants of vector competence is important for basic knowledge of virus-vector interactions and development of new interdiction strategies to control disease. Significant progress has been made towards identification of viral determinants of transmission, but the interacting molecules in vectors remain largely elusive. For negative-sense RNA viruses, vector factors that mediate the transmission process have not been well characterized.

Bunyavirales is the largest order of negative-sense RNA viruses; twelve families are described (http://www.ictvonline.org/virustaxonomy.asp). The *Bunyavirales* contains plant and insect vector-infecting viruses that make up the Family *Tospoviridae* (3-5). Within this family, there are eighteen species and several unassigned viruses that most likely will be classified as unequivocal members of the *Orthotospovirus* genus. *Tomato spotted wilt orthotospovirus* is the type species within this genus and has been best characterized in terms of viral host range, genome organization and protein functions (6, 7).

Tomato spotted wilt virus (TSWV) infects both monocotyledonous and dicotyledonous plants encompassing more than 1,000 plant species worldwide (8). Due to the extremely wide host range, TSWV has caused severe economic losses to various agricultural, vegetable and ornamental crops. The TSWV virion has a double-layered, host-derived membrane studded with two glycoproteins (G_N and G_C) on the surface. The viral glycoproteins play an essential

role in attachment to the thrips gut and fusion of the virus and host membrane (7, 9-11). Virus particles range in size from 80 to 120 nm in diameter, and inside the particle are three genomic RNAs designated long (L), medium (M) and small (S) RNA based on the relative size of each molecule.

Although TSWV can be maintained in the laboratory through mechanical inoculation, it is transmitted in nature by insect vectors commonly known as thrips (Order Thysanoptera, Family *Thripidae*). Five species of *Frankliniella* and two species of *Thrips* are reported to be the vectors of TSWV (6). Among these species, the western flower thrips, *Frankliniella occidentalis* Pergande, is the most efficient vector of TSWV and it has a worldwide distribution. TSWV is transmitted by thrips vectors in a persistent propagative manner, and the midgut cells and primary salivary glands are two major tissues for TSWV replication (12, 13). Only thrips that acquire virus during the early larval stage are inoculative as adults (13-15). Because the TSWV G_N protein has been identified to bind to thrips midguts and play a role in virus acquisition by thrips (9-11), we sought to identify thrips proteins that interact directly with G_N, the viral attachment protein (16). Using gel overlay assays to identify first instar larval (L1) proteins that bind to purified virions or G_N, we discovered six TSWV-interacting proteins (TIPs) from *F. occidentalis*. Identification of these proteins using mass spectrometry was followed with secondary assays to validate the interactions and characterize protein expression in larval thrips. Two TIPs, an endocuticle structural glycoprotein and cyclophilin, interacted with G_N and co-localized with G_N when co-expressed in insect cells. These thrips proteins may play a role in virus entry or mediate other steps in the virus infection process in thrips. These proteins represent the first thrips proteins that bind to TSWV proteins, and these discoveries provide insights toward a better understanding of the molecular interplay between vector and virus.

95

96 # Results

97 **Identification of bound *F. occidentalis* larval proteins using overlay assays**

98 Proteins extracted from first instar larvae bodies were separated by 2-D electrophoresis,
99 and overlay assays were performed with purified TSWV virions or recombinant G_N
100 glycoprotein to identify bound thrips proteins. Virion overlays identified a total of eight
101 proteins spots (Fig. 1) - three occurred consistently in all four biological replicates, while five
102 were present in three. Mass spectrometry and subsequent peptide sequence analysis against a
103 454-transcriptome database (*Fo* Seq) identified one to four different transcript matches per
104 spot (Table 1), where in four cases, the same putative transcript matched peptides in more
105 than one spot. Using recombinant G_N glycoprotein, 11 protein spots were detected in both
106 biological replicates of the overlay assay (Fig. 2), and each spot was comprised of a single
107 protein (single transcript match) occurring in multiple spots - there were a total of two
108 different G_N-interacting proteins represented by the 11 spots (Table 2). For each overlay
109 experiment that was run, a control blot was included to identify background, *i. e.*, non-
110 specific binding by the primary and secondary antibodies, demonstrating detection of the
111 positively identified spots well-exceeded background (Fig. 1 and 2). In an additional gel
112 overlay assay using virus-free plant extract (mock purification) obtained from healthy *D.*
113 *stramonium* plants, no protein spots above the antibody control were detected (data not
114 shown).

115

116 **Annotation of six candidate TSWV-interacting proteins (TIPs)**

117 Our stringent sequence-filtering criteria retained four different virion-interacting proteins
118 [endocuticle structural glycoprotein: endoCP-V (contig01248, GenBank accession:

MH884756); cuticular protein: CP-V (CL4900Contig1, MH884758), cyclophilin (CL4854Contig1, MH884760), and enolase (CL4706Contig1, MH884759), Table 1] and two G_N-interacting proteins [mitochondrial ATP synthase α, mATPase (CL4310Contig1, MH884761) and endocuticle structural glycoprotein; endoCP-G_N (CL4382Contig1, MH884757), Table 2] to move forward to validation and biological characterization. Collectively, these six protein candidates are referred to as 'TSWV-Interacting Proteins' or TIPs and their putative identifications and sequence features are shown in Table 3. Blastp analysis of the predicted, longest complete ORFs confirmed their annotations and putative sequence homology to proteins in other insects. The three cuticle-associated TIPs (endoCP-G_N, endoCP-V, and CP-V) contained predicted signal peptide sequences, indication of secreted proteins, and a chitin-binding domain (CHB4). Pairwise alignments (Blastp) between the translated ORFs of the three cuticle TIPs and the six other gel overlay-resolved CPs or endoCPs revealed sequence diversity; where matches among the different cuticle proteins occurred (cut-off = $E < 10^{-3}$) , % amino acid identities ranged from 53% – 67%, covering 30% – 49% of the queries, with e-values ranging from 2.4×10^{-2} – 3.6×10^{-24}. The only exception was the CP-V and contig00018 alignment, which appeared to be 100% identical along the entire length of contig00018 ($E = 2.6 \times 10^{-162}$) (data not shown). The other three TIPs (cyclophilin, enolase and mATPase) contained motifs characteristic of these proteins (Table 3).

Classification of cuticular TIPs

All three cuticular TIPs were classified as members of the Cuticle Protein - R&R Consensus motif (CPR) family (17) based on the occurrence of one RR extended consensus CHB4, with both endoCP-G_N ($E = 4 \times 10^{-18}$) and endoCP-V ($E = 1 \times 10^{-26}$) predicted to belong to the RR1 group, and CP-V weakly supported ($E = 5 \times 10^{-6}$) to belong to the RR2 group of CPRs. All three sequences were phylogenetically placed into the RR1 major clade

144 with strong bootstrap support (82%, Fig. S1) in relation to other *F. occidentalis* CPRs
145 previously found to be downregulated in TSWV-infected first instar larvae (18) and CPRs of
146 other insect species. Within the RR1 clade, the CP-V CHB4 domain clustered with a CP of
147 the small brown planthopper, *Laodelphax striatella* (KC485263.1, CprBJ), reported to bind to
148 the nucleocapsid protein pc3 of rice stripe virus (RSV) during infection of the vector (19) and
149 which was predicted ($E = 5 \times 10^{-7}$) to be classified in the RR1 group.
150
151 **Antisera show specificity against each TIP-peptide**

152 The antisera specifically bound to their TIP peptides in dot-blot assays (Fig. 3), although the
153 affinity of each antibody to its cognate TIP peptide varied. The mATPase antibody had
154 highest affinity to mATPase peptide, while the CP-V antibody had lowest affinity to CP-V
155 peptide (the high concentration of CP-V peptide, 2.5 mg/mL was used, and all primary and
156 secondary antibody incubation time was doubled, and the developing time for
157 chemiluminescence detection was increased). This result demonstrates the specificity of the
158 TIP-peptide antibodies that were used in subsequent localization experiments with first instar
159 thrips larvae.

160 ***In vivo* localization of TIPs in *F. occidentalis* in midguts and salivary glands**

161 Specific antisera raised against each confirmed TIP was used in immunolabeling
162 experiments to localize protein expression in L1 tissues *in vivo*. Visualization by confocal
163 microscopy revealed that all six TIPs were primarily localized at the foregut (esophagus),
164 midgut (epithelial cells and visceral muscle), salivary glands (including both primary and
165 tubular salivary glands), and Malpighian tubules (Fig. 4), and this was the case in 100% of
166 the dissected tissues treated with TIP-specific antisera. It was difficult to completely dissect
167 and separate hindgut from the carcass without damaging the tissue, therefore, the localization
168 of TIPs in the hindgut was unclear. For each experimental replicate and unique antibody,

169 controls of secondary antibody only and pre-immune serum plus secondary antibody were
170 conducted and visualized by confocal microscopy. The confocal laser settings (power and
171 percent/gain) were adjusted to remove any background fluorescence observed with pre-
172 immune serum for each TIP as they showed slightly higher background compared to the
173 secondary antibody control. The bright field and merged images of these controls, depicting
174 actin- and nuclei-labeling, are shown in Fig. S2.
175

176 **Validation of interactions between TIPs and TSWV G_N using BiFC**

177 Before launching a BiFC analysis of candidate protein interactions *in planta*, it is critical
178 to determine if position of a fused fluorescent protein tag (N- or C-terminus of the candidate
179 protein) affects the expression and/or localization of the fusion protein in cells. Furthermore,
180 it was expected that the signal peptides located on the N-terminus of the soluble (G_N-S) and
181 insoluble (G_N) TSWV glycoprotein, and the cuticular TIPs (CP-V, endoCP-V, endoCP-G_N),
182 would preclude placement of tags at the N-terminus of these proteins. GFP fused to the N-
183 terminus of the glycoprotein (G_N and G_N-S), the cuticle TIPs (endoCP-G_N and endoCP-V),
184 and mATPase α produced weak signal or reduced mobility in the cell (data not shown). For
185 the remaining proteins, there was no effect of fluorescent-protein tag location on protein
186 expression or mobility. Thus, all protein localization and BiFC validation experiments were
187 performed with C-terminally fused TIPs for consistency in the assays.

188 The GFP-TIP fusions displayed distinct cellular localization patterns when expressed in
189 plants (Fig. S3). Cyclophilin and mATPase appeared to be localized to the nuclei and along
190 the cell periphery, while enolase and CP-V were present in the membranes surrounding the
191 nuclei as well as the cell periphery. Both endoCP-G_N and endoCP-V had a punctate
192 appearance outside of the nucleus. All three cuticular TIPs (CP-V, endoCP-G_N, endoCP-V)
193 formed small bodies that appeared to be moving along the endo-membranes of the cell,

consistent with secretion. All TIPs were co-localized with the ER marker; however, none appeared to be co-localized with the Golgi marker (data not shown).

BiFC analysis validated the TSWV-TIPs interactions identified in the overlay assays between virions and G_N and enolase, m-ATPase, endoCP-G_N and endoCP-V (Fig. 5). We used the soluble form of the viral glycoprotein (G_N-S) and the insoluble form with the transmembrane domain and cytoplasmic tail in BiFC assays. The insoluble form of G_N interacted with enolase, endoCP-G_N and endoCP-V. The proposed ectodomain of G_N-S interacted with mATPase and endoCP-V. All of the BiFC interactions were detected in the membranes surrounding the nuclei and at the cell periphery, generally consistent with the localization patterns of the GFP-fused TIPs as described for the localization experiment above (Fig. S3).

Validation of gel overlay protein-protein interactions using the split-ubiquitin membrane-based yeast two-hybrid analysis

The split-ubiquitin membrane-based yeast two-hybrid (MbY2H) system was used to validate the gel overlay interactions between the six candidate TIPs and TSWV glycoprotein G_N. The presence of a transmembrane domain near the C-terminus of TSWV G_N makes the MbY2H system the best choice for validation of TSWV G_N interactions with the candidate TIPs. The interaction between G_N and endoCP-G_N was consistent and strong based on the number of colonies growing on QDO, *i.e.*, - more than 1,000 colonies on all QDO plates for all three replicates (Fig 6A), and this interaction was confirmed by β-galactosidase assay (Table S1). We detected a consistent but weak interaction (average of 15 colonies) between G_N and cyclophilin, and seven of nine colonies tested by β-galactosidase assay were positive. The remaining four TIPs showed no interaction with G_N using MbY2H. Contrary to the MbY2H results, G_N was determined to interact with enolase and endoCP-V in BiFC experiments. The steric constraints imposed by the position (C- or N-terminus) of the reporter

in the MbY2H (Ubiquitin half) and BiFC (YFP half) systems in yeast versus plants cells, respectively, may explain the contrasting interactions observed in these assays.

The non-conserved region of endoCP-G_N binds TSWV G_N

Given the role of G_N as the viral attachment protein in the larval thrips midgut epithelium (7, 10) and the confirmed direct interaction between endoCP-G_N and TSWV G_N, there was interest in broadly identifying the amino acid region in the endoCP-G_N sequence that binds G_N. We hypothesized that the non-conserved region of endoCP-G_N (N-terminal region up to 176 aa or 189 aa) and not the CHB4 motif might play an important role in the interaction with TSWV G_N. Using the MbY2H system, it was determined that the non-conserved region of the endoCP-G_N sequence had as strong of an interaction with TSWV G_N as the complete endoCP-G_N sequence (Fig 6B and Table S1) - more than 500 colonies on each QDO plate for each experimental replicate – while the predicted CHB4 motif alone (amino acid positions 190-284) or CHB4 plus few amino acids upstream (position 177-284) did not show an interaction. The non-conserved endoCP-G_N sequence region was determined to have no significant matches to sequences in NCBI non-redundant nucleotide and protein databases.

Cyclophilin and endoCP-G_N co-localized with TSWV G_N in insect cells

To further explore the interactions between TSWV G_N and the two robust thrips interacting proteins, cyclophilin and endoCP-G_N, we co-expressed the proteins as fusions with GFP or RFP in insect cells. The fusion proteins cyclophilin-RFP and endoCP-G_N-RFP and TSWV G_N-GFP were expressed individually and together in Sf9 cells. When fusion proteins cyclophilin-RFP and endoCP-G_N-RFP were individually expressed in Sf9 cells, they were localized within the entire cytoplasm (Fig. 7). Similarly, the fusion protein TSWV-G_N-GFP was also expressed in the cytoplasm, but specifically localized at structures that may be ER and/or Golgi, consistent with previous work localizing G_N to these organelles in animal

cells (20). When cyclophilin-RFP and TSWV-G_N-GFP or endoCP-G_N-RFP and TSWV-G_N-GFP were co-expressed in Sf9 cells, they co-localized within small punctate structures, which was different from their original localization (Fig. 7). However, the controls of co-expressed RFP and GFP (co-transfection of pHRW and pHGW) were distributed throughout the cytoplasm, and the localization of cyclophilin-RFP, endoCP-G_N-RFP and TSWV G_N-GFP did not change with the presence of GFP or RFP (Fig. S4). The controls of co-expressed RFP and GFP (co-transfection of pHRW and pHGW) were distributed throughout the cytoplasm in single and double transfections (Fig. 7). Although these unknown co-localization sites need to be further characterized, these co-localization results strongly supports the validity of *in vivo* interactions of cyclophilin and endoCP-G_N with TSWV-G_N.

Discussion

With the creation of transcriptome sequence resources for *F. occidentalis* and improved proteomics technologies, we have identified the first thrips proteins that bind directly to the TSWV attachment protein, G_N. With particular relevance to viral attachment to and internalization in epithelia, two TIPs (endocuticle structural glycoprotein, endoCP-G_N and cyclophilin) were confirmed to interact directly with G_N and were abundant in midgut and salivary gland tissues (21). These data may be the first indication of a protein(s) that serves 'receptor-like' roles in transmission biology of the tospoviruses. We narrowed down the G_N-binding region to the amino terminal region of endoCP-G_N excluding the conserved CHB4 domain, setting the stage for future work to decipher the essential amino acids within the non-conserved region necessary to establish the interaction. Three of the TIPs (mATPase, endoCP-V, and enolase) were validated to interact with G_N in BiFC assays, but not in MbY2H assays. With regards to other virus activities in host cells, the confirmed affinity of

268 G_N with diverse thrips proteins indicates that these insect proteins may be host factors
269 involved in steps in the virus infection cycle in the invertebrate host such as viral replication
270 and/or virion maturation previously observed in both the animal (22, 23) and plant hosts (24,
271 25). Technical limitations preclude functional analysis of the TIPs in acquisition of virus by
272 larval thrips. Knockdown (RNA interference) and knockout (genome editing) methods have
273 not been developed for larval thrips, even though RNA interference methods have been
274 developed to effectively knockdown genes in the much larger adult female thrips by delivery
275 of dsRNA directly into the hemocoel (26). Using currently available methods, larval thrips do
276 not survive the dsRNA-injection process, and even if successful, knockdown would be
277 delayed thus missing the narrow window of virus acquisition during the early larval
278 development.

279 The most enriched thrips proteins in the initial screen for those bound to virions or G_N
280 (Table 1 and 2, 72%) were cuticular proteins. Cuticular proteins are well characterized as
281 major components of insect hard and soft cuticles (27, 28). Soft cuticles have been
282 documented to line the insect foregut and hindgut (29, 30), and a transmission electron
283 microscopy study documented cuticle lining of the accessory and primary salivary gland (SG)
284 ducts of *F. occidentalis* (31). *In silico* sequence analysis of the three cuticular TIPs (CP-V,
285 endoCP-V, endoCP-G_N) revealed conserved CHB4 domains (R&R) suggesting their binding
286 affinity to chitin (heteropolymer of N-acetyl-β-D-glucosamine and glucosamine), also a
287 major component of cuticles and peritrophic membranes (PM) lining the midgut epithelium
288 of most insects (32). Hemipteran and thysanopteran midguts lack PMs, and are instead lined
289 with perimicrovillar membranes (PMM) (33, 34) - these structures have been reported to
290 contain lipoproteins, glycoproteins and carbohydrates (35, 36) and more recently, one study
291 documented the occurrence and importance of chitin in the PMM of *Rhodnius prolixus*
292 (kissing bug) midguts, marking the first hemipteran midgut reported to contain chitin (37).

293 Since all three cuticular TIPs were highly expressed in the midgut and SGs of larval *F.*
294 *occidentalis* in the present study, we hypothesize that chitin or chitin-like structures may
295 impregnate the thrips PMM and SG-linings, forming a matrix with endoCPs - however, this
296 remains to be empirically determined. Alternatively, the thrips TIPs annotated as cuticle
297 proteins with predicted chitin-binding domains may have yet-undescribed functions in insect
298 biology.

299 Cuticular proteins are emerging as important virus interactors and responders in diverse
300 vector-borne plant virus systems. A CP of the hemipteran vector, *Laodelphax striatellus*, was
301 found to interact with the nucleocapsid protein (pc3) of *Rice stripe virus* (genus *Tenuivirus,*
302 family *Phenuiviridae*) and was hypothesized to be involved in viral transmission and to
303 possibly protect the virus from degradation by a host immune response in the hemolymph
304 (19). Recently, a CP of another hemipteran vector, *Rhopalosiphum padi*, was identified to
305 interact with *Barley yellow dwarf virus*-GPV (genus *Luteovirus*, family *Luteoviridae*)
306 readthrough protein, and the gene transcript of this particular CP was differentially expressed
307 in viruliferous compared to virus-free aphids (38). At the transcript level, thrips cuticular
308 proteins of different types - including the thrips CPRs used in the present study to
309 phylogenetically place the three cuticular TIPs - were identified to be downregulated in
310 TSWV-infected first instar larvae (18). Although the three cuticular TIPs identified in the
311 present study were not reported in the previous study to be differentially-responsive to virus,
312 both implicate cuticle-associated proteins during the early infection events of TSWV in the
313 thrips vector.

314 Cyclophilins, also known as peptidyl-prolyl cis-trans isomerases, are ubiquitous proteins
315 involved in multiple biological processes, including protein folding and trafficking, cell
316 signaling, and immune responses (39). They have also been shown to promote or prevent
317 virus infection (40, 41), for example, cyclophilin A was found to bind to viral RNA to inhibit

318 replication of *Tomato bushy stunt virus* (genus *Tombusvirus*, family *Tombusviridae*) in plant
319 leaf cells (42), while cyclophilins of the aphid vector *Schizaphis graminum* have been shown
320 to play an important role in *Cereal yellow dwarf virus* (genus *Polerovirus*, family
321 *Luteoviridae*) transmission (43). Interactions between the thrips cyclophilin TIP (with G_N)
322 documented in the present study may affect similar virus processes, such as virus replication
323 and maturation, or thrips transmission and vector competence (43, 44). The same cyclophilin
324 was determined to be down-regulated in *F. occidentalis* first instar larvae during TSWV
325 infection (45), adding to the body of evidence that viruses modulate expression of
326 cyclophilins (46-51). The cyclophilin interaction with G_N was consistent but weak and this
327 may be the reason that it was not observed in the BiFC experiments. Alternative explanations
328 for the discrepancy in the cyclophilin-G_N interaction include: the interaction does not occur in
329 plant cells or that the weak interaction was not strong enough to fluoresce over the
330 background to detect an *in planta* interaction. Others have proposed that negative strand virus
331 matrix proteins – structural proteins that package viral RNA - evolved from cyclophilins (52);
332 however, bunyaviruses do not encode a matrix protein. One hypothesis for the direct
333 interaction between the cyclophilin with G_N may be to facilitate RNP packing into the virus
334 particle, perhaps serving as a surrogate matrix protein for TSWV.

335 Like cyclophilins, enolases of diverse hosts have been identified as both responsive to
336 and interactive partners with viruses. In general, enolases are essential metalloenzymes that
337 catalyze the conversion of 2-phosphoglycerate (2-PGE) to phosphoenolpyruvate (PEP) in the
338 glycolytic pathway for energy metabolism (53). Some are matrix metalloproteases known to
339 cleave cell surface receptors, modulate cytokine or chemokine activities, or release apoptotic
340 ligands by degrading all types of extracellular matrix proteins, such as collagen, elastin,
341 fibronectin, laminin, gelatin, and fibrin (54). The enolase TIP identified in the present study
342 was previously reported to be up-regulated in L1 bodies infected with TSWV (45), as was the

343 case for enolase in response to RSV in bodies of the planthopper vector, *L. striatellus* (55). In
344 the case of flaviviruses, *Aedes aegypti* enolase was shown to directly interact with purified
345 virus and recombinant envelope GP of dengue virus (56) and West Nile virus envelope
346 protein (57). The localization of this enolase in brush border membrane vesicles of this
347 mosquito species (58) strengthens the case for a proposed receptor role in virus entry into
348 vector mosquito midguts. Other insect-virus studies have proposed a role for enolase in
349 antiviral defense (54) and tracheal basal laminal remodeling aiding in virus escape from the
350 gut (59). If remodeling of the midgut basal lamina via enolase interactions occurs in TSWV-
351 infected larval thrips, that could be one hypothesis supporting dissemination of TSWV from
352 the larval midgut into the principal SGs (15).

353 The other TIP known to play a role in energy production is mitochondrial ATP synthase
354 α subunit. The multi-subunit enzyme mATPase is responsible for generating the majority of
355 cellular ATP required by eukaryotes to meet their energy needs. As with the other non-
356 cuticle TIPs, mATPase α subunit was previously identified to be differentially-abundant (up-
357 regulated) under TSWV infection (45), as was the case for RSV-infected *L. striatellus* vector
358 planthoppers (55). Mitochondria have also been previously implicated in virus-host biology.
359 For example, *African swine fever virus* (genus *Asfivirus*, family *Asfarviridae*) has been shown
360 to induce migration of mitochondria to the periphery of viral factories (60), possibly
361 suggesting that mitochondria supply energy for viral morphogenetic processes. The finding
362 that two TIPs in the present study have ontologies in energy production and metabolism
363 suggests that perturbation or direct interactions with these host proteins may be required for
364 the successful infection of *F. occidentalis* by TSWV.

365 The discovery of six TIPs is a significant step forward for understanding thrips
366 interactions with tospoviruses. The first evidence of TSWV protein-thrips protein interactions
367 was presented 20 years ago (61) and the proteins described herein are the first thrips proteins

documented to interact directly with the viral glycoprotein, G_N, involved in virus attachment to the midgut epithelial cells of the insect vector. In other eukaryotes, the six interacting proteins have biological functions that point to their putative roles in facilitating the virus infection/replication cycle by acting as a receptor or other essential step in the virus life cycle and/or host-response via a defense mechanism. The virus-host systems that have defined functions for analogous TIPs include plant viruses, arboviruses, and animal/human viruses, and the findings described here provide a framework for further exploration and testing of new hypotheses regarding their roles in TSWV-thrips interactions.

Materials and methods

Insect rearing and plant and virus maintenance

The *F. occidentalis* colony was established from insects collected on the island of Oahu, HI, and was maintained on green beans (*Phaseolus vulgaris*) at 22ºC (± 2ºC) under laboratory conditions as previously described (62). Thrips were age-synchronized based on their developmental stages. For the localization and bimolecular fluorescence complementation (BiFC) experiments, wildtype and transgenic *Nicotiana benthamiana* expressing CFP:H2B or RFP:ER (63) were grown in a growth chamber at 25ºC with a 14-hour light at 300 μM intensity and 10-hour dark cycle. TSWV (isolate TSWV-MT2) was maintained by both mechanical inoculation and thrips transmission using *Datura stramonium* and *Emilia sonchifolia*, respectively (12). To avoid generation of a virus isolate with an insect transmission deficiency, the virus was mechanically passaged only once. The single-pass mechanically-inoculated symptomatic *D. stramonium* leaves were used for insect acquisition of TSWV. Briefly, synchronized *F. occidentalis* first instar larvae (0-17-hour old) were collected and allowed an acquisition access period (AAP) on *D. stramonium* for 24 hours. After acquisition, *D. stramonium* leaves were removed and these larvae were maintained on

392 green beans until they developed to adults. Viruliferous adults were transferred onto clean *E.*
393 *sonchifolia* for two days. After inoculation, thrips and inoculated *E. sonchifolia* plants were
394 treated with commercial pest strips for two hours before the plants were moved to the
395 greenhouse for TSWV symptom development. The thrips-transmitted, TSWV symptomatic
396 *E. sonchifolia* leaves were only used for mechanical inoculation.

397 **TSWV purification**

398 Mechanically inoculated *D. stramonium* leaves were used for TSWV purification via
399 differential centrifugation and a sucrose gradient. Symptomatic leaves were homogenized
400 in extraction buffer (0.033 M KH_2PO_4, 0.067 M K_2HPO_4, and 0.01 M Na_2SO_3) in a 1:3
401 ratio of leaf tissue to buffer. The homogenate was then filtered through four layers of
402 cheesecloth, and the flow through was centrifuged at 7,000 rpm (7,445 *g*) for 15 min using
403 the Sorvall SLA 1500 rotor. To remove the cell debris, the pellet was resuspended in 65
404 mL 0.01 M Na_2SO_3 and was centrifuged again at 8,500 rpm (8,643 *g*) for 20 min using the
405 Sorvall SS34 rotor. The supernatant that contained the virions was centrifuged for 33 min
406 at 29,300 rpm (88205 *g*) using the 70 Ti rotor, and the pellet was resuspended in 15 mL
407 0.01 M Na_2SO_3 followed by another centrifugation at 9,000 rpm (9,690 *g*) for 15 min using
408 the Sorvall SS34 rotor. The centrifugation series was repeated one additional time. The
409 pellet was resuspended and loaded on a sucrose gradient (10 to 40% sucrose), which was
410 centrifuged for 35 min at 21,000 rpm (79,379 *g*) using the SW28 rotor. The virion band
411 was collected and centrifuged for 1 hour at 29,300 rpm (88,205 *g*) using the 70 Ti rotor.
412 The pellet was resuspended in 100 to 200 µl of 0.01 M Na_2SO_3. All centrifugation steps
413 were performed at 4ºC to prevent virion degradation. The purified virus was quantified
414 using the bicinchoninic acid (BCA) protein assay kit (ThermoFisher Scientific, Waltham,
415 MA, USA) following the manufacturer's instructions.

F. occidentalis L1 total protein extraction, quantification and two-dimensional (2-D) electrophoresis

Total proteins from age-synchronized healthy larval thrips (0-17-hour old) were extracted using the trichloroacetic acid-acetone (TCA-A) method (64, 65). Briefly, whole insects were ground using liquid nitrogen, and were dissolved in 500 µl TCA-A extraction buffer (10% of TCA in acetone containing 2% β-mercaptoethanol). This mixture was incubated at -20ºC overnight and centrifuged at 5,000 *g*, 4ºC for 30 min. After 3 washes with ice-cold acetone then air-drying, the pellet was resuspended in 200 µl General-Purpose Rehydration/Sample buffer (Bio-Rad Laboratories, Hercules, CA, USA). The suspension was centrifuged at 12,000 *g* for 5 min and the protein supernatant was quantified using the BCA protein assay kit (ThermoFisher Scientific) following manufacturer's instructions. For each gel, 150 µg of total protein extract was applied to an 11-cm IPG strip (pH 3–10) for isoelectric focusing (IEF). The IEF, IPG strip equilibration and second dimension separation of proteins were performed under the same conditions described by Badillo-Vargas et al (45).

Overlay assays

To identify thrips proteins that bind to TSWV virions and recombinant glycoprotein G_N, we conducted gel overlay assays. For the purified virion overlays, the experiment was performed four times (biological replications); and for the G_N overlay, the experiment was performed twice. For probing the protein-protein interactions, each unstained 2-D gel was electro-transferred onto Hybond-C Extra nitrocellulose membrane (Amersham Biosciences, Little Chalfont, UK) overnight at 30 V (4ºC) in protein transfer buffer (48 mM Tris, 39 mM glycine, 20% methanol, and 0.037% SDS). Then, the membrane was incubated with blocking buffer (PBST containing 0.05% Tween 20 and 5% dry milk) for 1h at room temperature on a rocker with a gentle rotating motion. Three different antigens were used to probe the thrips protein membranes: purified TSWV virions, recombinant glycoprotein G_N (*E. coli*

441 expressed), and virus-free plant extract from a mock virus purification (negative control). An
442 additional negative control blot (no overlay) treated with antibodies alone was included in
443 each overlay replicate. For the virus and G_N treatments, 25 µg/mL and 3.5 µg/mL of purified
444 TSWV virions and recombinant G_N glycoprotein, respectively, were incubated with
445 membranes in blocking buffer at 4ºC overnight with gentle rotating motion. Membranes were
446 washed three times using PBST and were incubated with polyclonal rabbit anti-TSWV G_N
447 antiserum at 1:2,000 dilution in blocking buffer for 2 hours at room temperature (9, 21).
448 After washing with PBST, membranes were incubated with HRP-conjugated goat-anti rabbit
449 antiserum at 1:5,000 dilution in blocking buffer for 1 hour at room temperature. The ECL
450 detection system (Amersham Biosciences) was used for protein visualization following the
451 manufacturer's instructions. The protein spots that were consistently observed on the
452 membranes were first compared with those proteins spots that interacted with antibody-only
453 blots (Fig 1A and Fig 2A) and virus-free plant extract blots, and then they were pinpointed
454 on the corresponding Coomassie Brilliant Blue G-250-stained 2-D gels for spot picking.

455 **Identification of TIPs**

456 Protein spots that were consistently identified in the 2-D gel overlays were selected and
457 manually picked for analysis. The picked proteins were processed and subjected to ESI mass
458 spectrometry as previously described (21). Protein spots (peptides) that had Mascot scores
459 (Mascot v2.2) with significant matches ($P \leq 0.05$) to translated *de novo*-assembled contigs
460 (all six frames) derived from mixed stages of *F. occidentalis* ("*Fo* Seq" 454-Sanger hybrid)
461 (45) were identified and NCBI Blastx was performed on the contigs to provisionally annotate
462 ($E < 10^{-10}$) the protein and to predict conserved motifs using the contig as the query and the
463 NCBI non-redundant protein database as the subject.

464 A second round of TIP candidate selection was conducted for stringency in moving
465 forward to cloning and confirmation of interactions. A contig sequence was retained if it

contained a complete predicted ORF (*i. e.*, presence of both start and stop codons predicted with Expasy, Translate Tool, http://web.expasy.org/translate/) and had at least 10% coverage by a matching peptide(s) identified for a spot as predicted by Mascot. *i. e.*, removal of proteins identified by a single peptide with less than 10% coverage to a *Fo* Seq contig and/or contigs with incomplete ORFs (lacking predicted stop codon). The translated ORFs were queried against the NCBI non-redundant protein database (Blastp), and CCTOP software (http://cctop.enzim.ttk.mta.hu) (66) and SignalP 4.1 Server (http://www.cbs.dtu.dk/services/SignalP/) (67) were used to predict the presence of transmembrane domains and signal peptides, respectively. Prosite (http://prosite.expasy.org/) was used to analyze putative post-translational modifications that may have affected electrophoretic mobility of identical proteins in the overlay assays, *i. e.*, same peptide sequence or *Fo* Seq contig match identified for more than one protein spot.

Classification and phylogenetic analysis of the three confirmed cuticular TIPs

Given the apparent enrichment of putative cuticular proteins (CP) identified in the overlay assays and the subsequent confirmation of three of those TIPs (CP-V, endoCP-G_N, endoCP-V), it was of interest to perform a second layer of protein annotations. The ORFs (amino acid sequence) of the three confirmed CP TIPs, 19 exemplar insect orthologous sequences obtained from NCBI GenBank, and a significant collection of structural CP transcripts previously reported to be differentially-expressed in TSWV-infected larval thrips of *F. occidentalis* (18) were subjected to two complementary arthropod CP prediction tools. CutProtFam-Pred (http://aias.biol.uoa.gr/CutProtFam-Pred/home.php) (68) was used to classify each amino acid sequence by CP family – there are 12 described families for arthropods, each distinguished by conserved sequence motifs shared by members (28) – and CuticleDB (http://bioinformatics.biol.uoa.gr/cuticleDB) (69) was used to distinguish what

was found to be two enriched, chitin-binding CP families in our dataset: CPR-RR1 and CPR-RR2, *i. e.*, R&R Consensus motif (17). The sequences flanking the RR1 and RR2 predicted chitin-binding domains were so divergent between the thrips CPs and across the entire set of CPs (thrips and other insects) that alignments using full-length ORFs were ambiguous and uninformative, thus illustrating the utility of the R&R Consensus for inferring evolutionary history of CP proteins. The flanking sequences were trimmed manually, and the R&R consensus sequences (RR1 and RR2) were aligned with MEGA7 (70) using ClustalW. Phylogenetic analyses were performed in MEGA7 using the Neighbor-Joining (NJ) method and the best substitution models determined for the data - Dayhoff matrix-based (71) or Jones Taylor Thorton (JTT) (72) methods for amino acid substitutions with Gamma distribution - to model the variation among sites. Bootstrap consensus trees (500 replicates) were generated by the NJ algorithm with pairwise deletion for handling gaps. The analysis involved 46 sequences and there were 95 amino acid positions in the final dataset.

Cloning of candidate TIPs and TSWV genes

For generation of full-length clones of TIPs that were used in various protein-protein assays, total RNA was extracted from L1 thrips (0-17-hour old) using 1 mL Trizol Reagent (ThermoFisher Scientific), then 200 µl chloroform and was precipitated with 500 µl isopropanol. The RNA pellet was dissolved in nuclease-free water, and 1µg total RNA was used for cDNA synthesis using the Verso cDNA Synthesis kit (ThermoFisher Scientific). The PCR was performed to amplify six identified TIP ORFs using high fidelity polymerase, FailSafe (Epicentre, Madison, WI, USA). The designed primers used are listed in Table S2. Amplicons were cloned into pENTR-D/TOPO (ThermoFisher Scientific).

TSWV genes were also cloned to pENTR-D/TOPO, then recombined to different vectors using Gateway cloning techniques. Coding sequences of different glycoprotein forms (soluble (G_N-S) and insoluble (G_N)) were amplified from pGF7 (73). Primers used for PCR

were listed in Table S2.

Polyclonal antisera against TIPs

To generate antibodies to the TIPs, the protein sequence was analyzed for multiple features such as antigenicity and hydrophobicity by the antibody manufacturer (GenScript, Piscataway, NJ), using the OptimumAntigen™ Design Tool (https://www.genscript.com/antigen-design.html). For each TIP, a 14 amino acid peptide was selected based on these predictions and by sequence alignments to other predicted protein sequences in GenBank. Due to the conserved CHB4 domain in endoCP-G_N, endoCP-V, and CP-V, the polyclonal antibodies against these three TIPs were generated using their non-conserved region. The peptides were synthesized, and all antisera were produced using mice (GenScript, Piscataway, NJ, United States). The peptide sequences for each TIP that were used for the antibody generation were: cyclophilin, LESFGSHDGKTSKK; enolase, ELRDNDKSQYHGKS; CP-V, TDSGQYRKEKRLED; endoCP-G_N, STKVNPQSFSRSSV; endoCP-V, VNPDGSFQYSYQTG; and mATPase, GHLDKLDPAKITDF.

Validation of antisera specificity against each TIP (peptide) using dot blot

Peptide antibodies to the six TIPs were generated by GenScript using their standardized work flow. For each TIP, the amino acids of highest antigenic potential were identified, peptides were synthesized, antibodies were generated by injection in mice, and antibodies were tested for reactivity and specificity using dot-blot assays. The peptides that were used to generate each antibody were diluted to 100 µg/mL using 1×PBS (pH=7.2), with the exception of the CP-V peptide that was diluted to 2.5 mg/mL (briefly explain why – lower sensitivity?). Two ul of each diluted peptide was spotted onto the same nitrocellulose membrane strip along with the controls of PBS and pre-immune serum (500,000 × dilution). A total of 6 membrane strips, one for each TIP-peptide antibody, were loaded with the same peptide

541 samples and controls. After membrane strips dried, each strip was incubated with blocking
542 buffer (5% non-fat milk in TBS-T), followed by incubation with the six different primary
543 antibodies (0.5 µg/mL, produced by GenScript), respectively. After three washes with TBS-T
544 (3×10 min), all membrane strips were incubated with secondary antibody, goat anti-mouse
545 IgG (H+L)-HRP conjugate (1:5,000 dilution, Bio-Rad Laboratories). After three washes with
546 TBS-T, the SuperSignal™ West Dura Extended Duration Substrate (ThermoFisher Scientific)
547 was added onto individual membrane strips. Each membrane strip was developed separately
548 for 5 to 10 min, however, the membrane strip that was incubated with the CP-V peptide
549 antibody was developed for 40 min. Then a picture was taken using iBright Imaging system
550 (CL1000, ThermoFisher Scientific). The blocking, primary and secondary antibody
551 incubation steps were incubated for 1 hour at room temperature, and the strip probed with
552 CP-V peptide antibody was incubated for 2 hours at room temperature. The entire experiment
553 was performed three times.

554 **Immunolabeling thrips guts, Malphigian tubules, and salivary glands**

555 To determine the location of TIPs expression in the most efficient thrips stage that
556 acquires TSWV (L1), we used the TIPs antibodies in immunolocalization experiments.
557 Treatments in the experiments included peptide antibodies to the TIPs and background
558 controls of dissected insects incubated with i) only secondary antibody and ii) insects treated
559 with pre-immune serum and secondary antibody. Newly emerged larvae (0-17-hour old)
560 were collected from green beans and were then fed on 7% sucrose solution for 3 hours to
561 clean their guts from plant tissues. The larvae were dissected on glass slides using cold
562 phosphate saline (PBS) buffer and Teflon coated razor blades. The dissected thrips were
563 transferred into 2-cm-diam., flat-bottomed watch glasses (U.S. Bureau of Plant Industry, BPI
564 dishes) and the tissues were fixed for 2 hours using 4% paraformaldehyde solution in 50 mM
565 sodium phosphate buffer (pH 7.0). The tissues were washed using PBS buffer after fixation

566 and were incubated with PBS buffer including 1% Triton X-100 overnight. The overnight
567 permeabilized tissues were then washed before incubation in blocking buffer which included
568 PBS, 0.1% Triton X-100 and 10% normal goat serum (NGS) for 1 hour. After removing the
569 blocking buffer, the dissected thrips were incubated with primary antibody, 100 µg/mL mice-
570 generated antisera against each individual TIP (GenScript) that was diluted in antibody buffer
571 (0.1% Triton X-100 and 1% NGS). After washing, 10 µg/mL secondary antibody, goat anti-
572 mouse antibody conjugated with Alexa Fluor 488 (ThermoFisher Scientific) was used to
573 incubate the dissected thrips organs. Incubation was performed at room temperature for 2.5
574 hours, 1x PBS buffer was used for washing and every wash step included three rinses, and
575 the secondary antibody incubation was protected from light by covering the samples with
576 aluminum foil. After removing antibodies and washing, dissected thrips were incubated for 2
577 hours with Phalloidin-Alexa 594 conjugated (ThermoFisher Scientific) in 1x PBS with a
578 concentration of 4 units/mL for actin staining. After washing, the tissues were transferred
579 onto glass slides, and SlowFade™ Diamond Antifade Mountant with DAPI (ThermoFisher
580 Scientific) was added onto tissues to stain the nuclei. The cover slips were slowly placed on
581 tissues to avoid bubbles, then sealed with transparent nail polish at the edges. After blocking,
582 the dissected thrips tissues that were only incubated with secondary antibody (without adding
583 primary antibody) and the tissues incubated with each pre-immune mouse antiserum
584 (GenScript) were used as negative controls, respectively. All the experiments were
585 performed twice.

586 Inherent with very small tissues (< 1 mm body size), there were common losses or
587 damaged tissues during the dissection process and staining procedures; so only the number of
588 visibly intact tissue that made it through to microscopic observation were used for data
589 collection and this number varied for each type of tissue (Table S4). The auto-fluorescent
590 background from thrips tissues incubated with each pre-immune antiserum and secondary

591 antibodies was slightly higher than the thrips tissues incubated with PBS buffer and
592 secondary antibodies (negative control) (data not shown), therefore, the confocal laser
593 settings (power and percent gain) were adjusted to remove any background fluorescence
594 observed for these treatments.

595 **Split-ubiquitin membrane-based yeast two-hybrid (MbY2H)**

596 The MbY2H system was used to validate TSWV G_N-TIPs interactions identified in the
597 gel overlay assays. The MbY2H system enables validation of interactions for soluble and
598 integral membrane proteins. TSWV G_N coding sequence were cloned into the MbYTH vector
599 pBT3-SUC, and the six TIP ORFs were cloned to vector pPR3N using the SfiI restriction site
600 (Dualsystems Biotech, Schlieren, Switzerland). To identify the region of endoCP-G_N that
601 binds to TSWV G_N using MbY2H, the amino acid sequence of endoCP-G_N (284aa) was used
602 to search against the NCBI non-redundant protein database using Blastp. The conserved
603 CHB4 domain was located at the C-terminus of endoCP-G_N (amino acid 190-246).
604 Therefore, the possible interacting domains, the non-conserved region of endoCP-G_N (1-
605 189aa) and the conserved CHB4 domain (190-274aa), were individually cloned into pPR3N
606 using the SfiI restriction site. Based on the Blastp results, the homologous sequences from
607 other insect species encompassed some additional amino acids upstream of the CHB4
608 domain; therefore, we made an alternative construct that included the conserved CBH4
609 domain starting from amino acid 177. Hence, the coding sequence of 1-176aa and 177-284aa
610 of endoCP-G_N were also cloned to pPR3N using the SfiI restriction site. Primers used for
611 cloning are listed in Table S3.

612 The MbY2H assays were performed using the manufacturer's instructions with
613 recombinant plasmids that were confirmed by Sanger sequencing. Yeast (strain NYM51)
614 competent cells were freshly prepared and recombinant bait plasmids, pBT3-SUC-G_N were
615 transformed into yeast cells. Briefly, 1.5 µg of bait plasmids were added into 100 µl of yeast

competent cells with 50 µg of denatured Yeastmaker Carrier DNA (Takara Bio USA, Mountain View, CA) and 500 µl PEG/LiAc. The mixture was incubated at 30ºC for 30 min with mixing every 10 min. Twenty µl of DMSO was then added into each reaction, and the cells were incubated at 42ºC for 20 min with mixing every 5 min. After centrifugation at 14,000 rpm for 15 sec, the supernatant was removed, and the pellet was resuspended in 1 mL of YPDA media. The re-suspended cells were incubated at 30ºC for 90 min with shaking at 200 rpm. Then, cells were centrifuged at 14,000 rpm for 15 sec, and resuspended in 500 µl of sterile 0.9% (w/v) NaCl, which was then spread and cultured on SD/–Trp dropout media at 30ºC until the colonies were visible. Several colonies from the same SD/–Trp plate were cultured for preparing yeast competent cells. Then each individual recombinant plasmid, pPR3N-TIP or pPR3N-partial endoCP-G_N (1.5 µg/transformation reaction), was transformed into yeast competent cells expressing fused Nub-G_N. The transformants were cultured on both SD/–Leu/–Trp double dropout (DDO) and SD/–Ade/–His/–Leu/–Trp quadruple dropout (QDO) media. The positive controls included transformation of pOst1-NubI into the yeast strain NYM51 that already expressed fused Nub-G_N or Nub-N, as well as co-transformation of pTSU2-APP and pNubG-Fe65 into the yeast strain NYM51. Transformation of pPR3N (empty vector) into the yeast strain NYM51 that already expressed fused Nub-G_N was used as the negative control. Interactions between G_N-Cub and NubI, G_N-Cub and NubG were used as positive and negative controls respectively. All transformants were spread and cultured on both DDO and QDO media and cultured at 30ºC in an incubator. The entire experiment was performed three times.

Yeast β-galactosidase assay

Expression of the reporter gene *LacZ* and the activity of expressed β-galactosidase in yeast cells derived from MbY2H was determined by a β-galactosidase assay kit following the manufacturer's protocol (ThermoFisher Scientific). Each yeast colony was transferred, mixed

with 250 µl of Y-PER by vortex, and their initial OD_{660} value was determined. After adding 250 µl 2X β-galactosidase assay buffer to the mixed solution, the reaction was incubated at 37ºC until the color change of solution was observed. Two hundred µl of β-galactosidase assay stop solution was added immediately into color change solution, and the reaction time was recorded. Cell debris was removed by centrifugation at 13,000 *g* for 30 seconds. Supernatant was transferred into cuvettes to measure OD_{420} using the blank including 250 µl of Y-PER reagent, 250 µl β-galactosidase assay buffer and 200 µl β-galactosidase assay stop solution. The β-galactosidase activity was calculated using the equation from the manufacturer's protocol.

GFP fusion protein expression and bimolecular fluorescence complementation (BiFC) in *Nicotiana benthamiana*

To visualize protein expression and localization in plants, TSWV G_N (ORFs G_N and G_NS) and TIP ORFs (mATPase, CP-V, endoCP-V, endoCP-G_N, cyclophilin and enolase) were expressed as fusions to autofluorescent proteins. They were moved from their entry clones into pSITE-2NB (GFP fused to the carboxy terminus of the protein of interest) or pSITE-2CA (GFP fused to the amino terminus of the protein of interest) using Gateway LR Clonase (74). After validation of plasmids by Sanger sequencing, they were transformed into *Agrobacterium tumefaciens* strain LBA 4404. The transformed LBA 4404 was grown for two days at 28ºC and re-suspended in 0.1 M MES and 0.1 M $MgCl_2$ to an OD_{600} between 0.6 to 1. After the addition of 0.1 M acetosyringone, the suspension was incubated at room temperature for two hours, and then infiltrated in transgenic *N. benthamiana* expressing an endoplasmic reticulum (ER) marker fused to the red fluorescent protein (m5RFP-HDEL) (63). Two days after infiltration, leaf tissue was mounted in water on a microscope slide for detection of GFP by confocal microscopy. Plants were infiltrated a minimum of two separate occasions with at least two leaves per plant in two different plants. A minimum of fifty cells

were visualized in each plant to confirm the localization patterns of the proteins *in planta*.

The preliminary localization results and sequence analysis informed the fusion construct design for BiFC assays. Signal peptides were identified in the amino terminus of G_N, and three TIPs (all cuticle proteins) and the signal peptide is required for proper localization and function of fusion-GFP/YFP proteins in *N. benthamiana* for BiFC assays. Based on the expression and localization results of GFP fusion proteins, we fused half YFPs (either amino or carboxy half of YFP) to the carboxy termini of all proteins with N-terminal signal peptides using BiFC plasmids pSITE-NEN and pSITE-CEN (63). All ORFS were transferred between plasmids using Gateway LR Clonase II Enzyme Mix (ThermoFisher Scientific). All clones were transformed into *A. tumefaciens* strain LBA 4404 and confirmed by Sanger sequencing.

Each combination of TIPs and TSWV G_N and G_N-S was infiltrated into *N. benthamiana* expressing CFP fused to a nuclear marker, histone 2B, (CFP-H2B) (63), and a minimum of three independent experiments with two plants and two leaves per plant for each combination of proteins. For the analysis of interactions, a minimum of 50 cells with similar localization patterns was required to confirm the interaction and a minimum of two separate images were captured on each occasion for documentation. GST fusions to YFP halves were utilized as a non-binding control for each of the TIPs. To be recorded as a positive interaction, fluorescence of the interacting TSWV protein-TIPs was required to be above that observed between each TIP and GST.

Laser scanning confocal microscopy

Confocal microscopy was used to detect the fluorescent signal produced from TIP antibody labelling in thrips tissues and BiFC experiments in plants. All images were acquired on a Zeiss LSM 780 laser scanning confocal microscope using the C-Apochromat 40x/1.2 W Korr M27 and Plan-Apochromat 20x/0.8 M27 objectives. Image acquisition was conducted on

690 Zen 2 black edition v. 10.0.0 at 1024 x 1024 pixels with a scan rate of 1.58 μs per pixel with
691 pixel average of 4-bit and 16-bit depth. The laser power and percent gain settings for
692 detection of nuclei and actin as well as the bright field were adjusted accordingly. Laser
693 power and percent gain settings for detection of TIPs were equal or smaller than their
694 controls. Z-stacks were taken for localization of TIPs in thrips. Eight (TIPs localization) Z-
695 stack slides were processed using Maximum intensity projection using Zen 2 black. Zen 2
696 blue edition lite 2010 v. 2.0.0.0 was used for image conversion to jpeg format.
697

698 **Co-localization of TIPs and TSWV G_N in insect cells**

699 The ORFs of cyclophilin, endoCP-G_N and TSWV G_N were cloned into pENTR/D-TOPO
700 (Thermo Fisher Scientific, Grand Island, NY). TSWV G_N was amplified by primers ENTR-
701 endoCP-G_NF and ENTR-TSWV-G_NR1353 (Table S2). The cyclophilin and endoCP-G_N
702 ENTR clones were recombined into pHWR, and the TSWV G_N ENTR clone was moved into
703 pHWG (*Drosophila* gateway collection, DGRC, Bloomington, Indiana). Both pHWR and
704 pHWG have Hsp70 promotor and gateway cloning cassette, and both RFP and GFP were
705 expressed at the C-terminus of TIPs or TSWV G_N.
706 The recombinant expression constructs were confirmed by Sanger sequencing and then
707 transfected into Sf9 cells. Single- or co-transfections were performed using Cellfectin II
708 Reagent (ThermoFisher Scientific) following the manufacturer's protocol. Briefly, Sf9 cells
709 were counted, diluted to 5×10^5, and then 2 ml aliquots were seeded into each well of a 6-well
710 plate. Eight μL of Cellfectin II reagent and 3 ng of each recombinant plasmid were diluted in
711 100 μL Grace's medium (Thermofisher Scientific), respectively. After vortex-mixing, both
712 diluted DNA and diluted Cellfectin II reagent were incubated at room temperature for 30 min
713 and then were combined and incubated for an additional 30 min. Another 800 μL of Grace's
714 medium was added into each DNA-lipid mixture, and the entire 1 mL solution was slowly

added onto Sf9 cells. The transfection mix was incubated for 5 hours at 27°C after which the solution was removed and replaced by 2 mL Sf-900 III medium. Single transfected plasmids were pHWR-cyclophilin, pHWR-endoCP-G_N and pHWG-TSWV G_N; co-transfected plasmids were pHWR-cyclophilin and pHWG-TSWV G_N; pHWR-endoCP-G_N and pHWG-TSWV G_N. To rule out non-specific interactions between the proteins of interests (TIPs or G_N) and the autofluorescent protein tags, they were co-transfected with unfused RFP or GFP. In addition, a mock (no DNA) transfection was also included as negative control.

After 72 h, Sf9 cells were resuspended and re-seeded in a 24-well glass bottom Sensoplate (Greiner Bio-One, Monroe, NC) with 1:2 dilution. The cells were stained with DAPI and then visualized by the Cytation 5 Cell Imaging Multi-Mode Reader with objectives 40x PL FL and 20x PL FL (BioTek, Winooski, VT). Image acquisition was performed with BioTek Gen 5 Microplate Reader and Imager Software, version 3.04. Images were captured using default settings. To detect GFP and RFP, the exposure settings (LED intensity/integration time/camera gain) of mock transfected cells were set up as the baseline and different treatments were set to no more than the mock settings. Other parameter settings for detection of nuclei and bright field were adjusted accordingly. The entire experiment was performed four times.

Data availability

The GenBank accession numbers for six TIPs are: cyclophilin, MH884760; enolase, MH884759; cuticular protein: CP-V, MH884758; endoCP-G_N, MH884757; endoCP-V, MH884756; mitochondrial ATP synthase α, MH884761.

Acknowledgements

We thank Thomas L. German and Ranjit Dasgupta for providing purified G_N-S for protein

overlays. This project was supported by the following grants: USDA-NIFA 2007-35319-18326 and 2016-67013-27492, USDA-FNRI 6034-22000-039-06S, and National Science Foundation CAREER Grant IOS-0953786. Ismael E. Badillo-Vargas was partially supported by the National Institute of Food and Agriculture Predoctoral Fellowship, grant KS602489.

References

1. Gubler DJ. 1998. Resurgent vector-borne diseases as a global health problem. Emerging infectious diseases 4:442-450.
2. Gubler DJ. 2002. The global emergence/resurgence of arboviral diseases as public health problems. Arch Med Res 33:330-342.
3. Beaty BJ, Bishop DH. 1988. Bunyavirus-vector interactions. Virus Res 10:289-301.
4. Elliott RM. 1997. Emerging viruses: the Bunyaviridae. Mol Med 3:572-577.
5. Horne KM, Vanlandingham DL. 2014. Bunyavirus-vector interactions. Viruses 6:4373-4397.
6. Rotenberg D, Jacobson AL, Schneweis DJ, Whitfield AE. 2015. Thrips transmission of tospoviruses. Curr Opin Virol 15:80-89.
7. Whitfield AE, Ullman DE, German TL. 2005. Tospovirus-thrips interactions. Annu Rev Phytopathol 43:459-489.
8. Parrella G, Gognalons P, Gebre-Selassie K, Vovlas C, Marchoux G. 2003. An update of the host range of Tomato spotted wilt virus. Journal of Plant Pathology 85:227-264.
9. Montero-Astua M, Rotenberg D, Leach-Kieffaber A, Schneweis BA, Park S, Park JK, German TL, Whitfield AE. 2014. Disruption of vector transmission by a plant-expressed viral glycoprotein. Mol Plant Microbe Interact 27:296-304.
10. Whitfield AE, Kumar NK, Rotenberg D, Ullman DE, Wyman EA, Zietlow C, Willis DK, German TL. 2008. A soluble form of the *tomato spotted wilt virus* (TSWV)

764 glycoprotein G_N (G_N-S) inhibits transmission of TSWV by *Frankliniella occidentalis*.
765 Phytopathology 98:45-50.
766 11. Whitfield AE, Ullman DE, German TL. 2004. Expression and characterization of a
767 soluble form of *tomato spotted wilt virus* glycoprotein G_N. J Virol 78:13197-13206.
768 12. Ullman DE, German TL, Sherwood JL, Westcot DM, Cantone FA. 1993. Tospovirus
769 replication in insect vector cells: immunocytochemical evidence that the nonstructural
770 protein encoded by the S RNA of tomato spotted wilt tospovirus is present in thrips
771 vector cells. Phytopathology 83:456-463.
772 13. Wijkamp I, van Lent J, Kormelink R, Goldbach R, Peters D. 1993. Multiplication of
773 tomato spotted wilt virus in its insect vector, *Frankliniella occidentalis*. J Gen Virol
774 74:341-349.
775 14. Nagata T, Inoue-Nagata AK, Smid HM, Goldbach R, Peters D. 1999. Tissue tropism
776 related to vector competence of *Frankliniella occidentalis* for tomato spotted wilt
777 tospovirus. J Gen Virol 80:507-515.
778 15. Ullman DE, Cho JJ, Mau RFL, Westcot DM, Custer DM. 1992. A midgut barrier to
779 tomato spotted wilt virus acquisition by adult western flower thrips. Phytopathology
780 82:1333-1342.
781 16. Sin SH, McNulty BC, Kennedy GG, Moyer JW. 2005. Viral genetic determinants for
782 thrips transmission of Tomato spotted wilt virus. Proc Natl Acad Sci U S A 102:5168-
783 5173.
784 17. Rebers JE, Riddiford LM. 1988. Structure and expression of a *Manduca sexta* larval
785 cuticle gene homologous to *Drosophila* cuticle genes. J Mol Biol 203:411-423.
786 18. Schneweis DJ, Whitfield AE, Rotenberg D. 2017. Thrips developmental stage-
787 specific transcriptome response to tomato spotted wilt virus during the virus infection
788 cycle in *Frankliniella occidentalis*, the primary vector. Virology 500:226-237.

19. Liu W, Gray S, Huo Y, Li L, Wei T, Wang X. 2015. Proteomic analysis of interaction between a plant virus and its vector insect reveals new functions of hemipteran cuticular protein. Mol Cell Proteomics 14:2229-2242.

20. Snippe M, Smeenk L, Goldbach R, Kormelink R. 2007. The cytoplasmic domain of tomato spotted wilt virus Gn glycoprotein is required for Golgi localisation and interaction with Gc. Virology 363:272-279.

21. Montero-Astua M, Ullman DE, Whitfield AE. 2016. Salivary gland morphology, tissue tropism and the progression of tospovirus infection in *Frankliniella occidentalis*. Virology 493:39-51.

22. Elliott RM, Schmaljohn CS. 2013. Bunyaviridae. *In* Knipe DM, Howley PM (ed), *Fields Virology*, 6th ed. Lippincott Williams & Wilkins, Philadelphia, PA.

23. Wang H, Alminaite A, Vaheri A, Plyusnin A. 2010. Interaction between hantaviral nucleocapsid protein and the cytoplasmic tail of surface glycoprotein Gn. Virus Research 151:205-212.

24. Ribeiro D, Borst JW, Goldbach R, Kormelink R. 2009. Tomato spotted wilt virus nucleocapsid protein interacts with both viral glycoproteins Gn and Gc *in planta*. Virology 383:121-130.

25. Richmond KE, Chenault K, Sherwood JL, German TL. 1998. Characterization of the nucleic acid binding properties of tomato spotted wilt virus nucleocapsid protein. Virology 248:6-11.

26. Badillo-Vargas IE, Rotenberg D, Schneweis BA, Whitfield AE. 2015. RNA interference tools for the western flower thrips, *Frankliniella occidentalis*. J Insect Physiol 76:36-46.

27. Andersen SO, Hojrup P, Roepstorff P. 1995. Insect cuticular proteins. Insect Biochem Mol Biol 25:153-176.

814 28. Willis JH. 2010. Structural cuticular proteins from arthropods: annotation,
815 nomenclature, and sequence characteristics in the genomics era. Insect Biochem Mol
816 Biol 40:189-204.
817 29. Chapman RF, Simpson SJ, Douglas AE. 2013. The Insects: Structure and Function,
818 5th ed. Cambridge University Press.
819 30. Maddrell SHP, Gardiner BOC. 1980. The permeability of the cuticular lining of the
820 insect alimentary canal. The Journal of Experimental Biology 85:227-237.
821 31. Ullman DE, Westcot DM, Hunter WB, Mau RFL. 1989. Internal anatomy and
822 morphology of *Frankliniella occidentalis* (Pergande) (Thysanoptera: Thripidae) with
823 special reference to interactions between thrips and tomato spotted wilt virus.
824 International Journal of Insect Morphology and Embryology 18:289-310.
825 32. Zhu KY, Merzendorfer H, Zhang W, Zhang J, Muthukrishnan S. 2016. Biosynthesis,
826 turnover, and functions of chitin in insects. Annu Rev Entomol 61:177-196.
827 33. Cristofoletti PT, Ribeiro AF, Deraison C, Rahbe Y, Terra WR. 2003. Midgut
828 adaptation and digestive enzyme distribution in a phloem feeding insect, the pea aphid
829 *Acyrthosiphon pisum*. J Insect Physiol 49:11-24.
830 34. Silva CP, Silva JR, Vasconcelos FF, Petretski MD, Damatta RA, Ribeiro AF, Terra
831 WR. 2004. Occurrence of midgut perimicrovillar membranes in paraneopteran insect
832 orders with comments on their function and evolutionary significance. Arthropod
833 Struct Dev 33:139-148.
834 35. Albuquerque-Cunha JM, Gonzalez MS, Garcia ES, Mello CB, Azambuja P, Almeida
835 JC, de Souza W, Nogueira NF. 2009. Cytochemical characterization of microvillar
836 and perimicrovillar membranes in the posterior midgut epithelium of *Rhodnius*
837 *prolixus*. Arthropod Struct Dev 38:31-44.
838 36. Terra WR, Costa RH, Ferreira C. 2006. Plasma membranes from insect midgut cells.

839 An Acad Bras Cienc 78:255-269.

840 37. Alvarenga ES, Mansur JF, Justi SA, Figueira-Mansur J, Dos Santos VM, Lopez SG,
841 Masuda H, Lara FA, Melo AC, Moreira MF. 2016. Chitin is a component of the
842 *Rhodnius prolixus* midgut. Insect Biochem Mol Biol 69:61-70.

843 38. Wang H, Wu K, Liu Y, Wu Y, Wang X. 2015. Integrative proteomics to understand
844 the transmission mechanism of *Barley yellow dwarf virus-GPV* by its insect vector
845 *Rhopalosiphum padi*. Sci Rep 5:10971.

846 39. Kumari S, Roy S, Singh P, Singla-Pareek SL, Pareek A. 2013. Cyclophilins: proteins
847 in search of function. Plant Signal Behav 8:e22734.

848 40. Liu H, Xue Q, Cao W, Yang F, Ma L, Liu W, Zhang K, Liu X, Zhu Z, Zheng H.
849 2018. Foot-and-mouth disease virus nonstructural protein 2B interacts with
850 cyclophilin A, modulating virus replication. FASEB J 32:6706-6723.

851 41. von Hahn T, Ciesek S. 2015. Cyclophilin polymorphism and virus infection. Curr
852 Opin Virol 14:47-49.

853 42. Kovalev N, Nagy PD. 2013. Cyclophilin A binds to the viral RNA and replication
854 proteins, resulting in inhibition of tombusviral replicase assembly. J Virol 87:13330-
855 13342.

856 43. Tamborindeguy C, Bereman MS, DeBlasio S, Igwe D, Smith DM, White F, MacCoss
857 MJ, Gray SM, Cilia M. 2013. Genomic and proteomic analysis of *Schizaphis*
858 *graminum* reveals cyclophilin proteins are involved in the transmission of *cereal*
859 *yellow dwarf virus*. Plos One 8:e71620.

860 44. Yang X, Thannhauser TW, Burrows M, Cox-Foster D, Gildow FE, Gray SM. 2008.
861 Coupling genetics and proteomics to identify aphid proteins associated with vector-
862 specific transmission of polerovirus (luteoviridae). J Virol 82:291-299.

863 45. Badillo-Vargas IE, Rotenberg D, Schneweis DJ, Hiromasa Y, Tomich JM, Whitfield

AE. 2012. Proteomic analysis of *Frankliniella occidentalis* and differentially expressed proteins in response to tomato spotted wilt virus infection. J Virol 86:8793-8809.

46. An P, Wang LH, Hutcheson-Dilks H, Nelson G, Donfield S, Goedert JJ, Rinaldo CR, Buchbinder S, Kirk GD, O'Brien SJ, Winkler CA. 2007. Regulatory polymorphisms in the cyclophilin A gene, *PPIA*, accelerate progression to AIDS. PLoS Pathog 3:e88.

47. Bleiber G, May M, Martinez R, Meylan P, Ott J, Beckmann JS, Telenti A. 2005. Use of a combined ex vivo/in vivo population approach for screening of human genes involved in the human immunodeficiency virus type 1 life cycle for variants influencing disease progression. Journal of Virology 79:12674-12680.

48. Chatterji U, Bobardt M, Selvarajah S, Yang F, Tang H, Sakamoto N, Vuagniaux G, Parkinson T, Gallay P. 2009. The isomerase active site of cyclophilin A is critical for hepatitis C virus replication. Journal of Biological Chemistry 284:16998-17005.

49. Kaul A, Stauffer S, Berger C, Pertel T, Schmitt J, Kallis S, Zayas M, Lohmann V, Luban J, Bartenschlager R. 2009. Essential role of cyclophilin A for hepatitis C virus replication and virus production and possible link to polyprotein cleavage kinetics. PLoS Pathog 5:e1000546.

50. Rits MAN, van Dort KA, Kootstra NA. 2008. Polymorphisms in the regulatory region of the Cyclophilin A gene influence the susceptibility for HIV-1 infection. PLoS One 3:e3975.

51. Yang F, Robotham JM, Nelson HB, Irsigler A, Kenworthy R, Tang H. 2008. Cyclophilin A is an essential cofactor for hepatitis C virus infection and the principal mediator of cyclosporine resistance in vitro. Journal of Virology 82:5269-5278.

52. Krupovic M, Koonin EV. 2017. Multiple origins of viral capsid proteins from cellular ancestors. Proc Natl Acad Sci U S A 114:E2401-E2410.

889 53. Brown JR, Doolittle WF. 1997. Archaea and the prokaryote-to-eukaryote transition.
890 Microbiology and Molecular Biology Reviews 61:456-502.
891 54. Van Lint P, Libert C. 2007. Chemokine and cytokine processing by matrix
892 metalloproteinases and its effect on leukocyte migration and inflammation. J Leukoc
893 Biol 82:1375-1381.
894 55. Zhang F, Guo H, Zheng H, Zhou T, Zhou Y, Wang S, Fang R, Qian W, Chen X.
895 2010. Massively parallel pyrosequencing-based transcriptome analyses of small
896 brown planthopper (*Laodelphax striatellus*), a vector insect transmitting rice stripe
897 virus (RSV). BMC Genomics 11:303.
898 56. Munoz Mde L, Limon-Camacho G, Tovar R, Diaz-Badillo A, Mendoza-Hernandez G,
899 Black WCt. 2013. Proteomic identification of dengue virus binding proteins in *Aedes*
900 *aegypti* mosquitoes and *Aedes albopictus* cells. Biomed Res Int 2013:875958.
901 57. Colpitts TM, Cox J, Nguyen A, Feitosa F, Krishnan MN, Fikrig E. 2011. Use of a
902 tandem affinity purification assay to detect interactions between West Nile and
903 dengue viral proteins and proteins of the mosquito vector. Virology 417:179-187.
904 58. Popova-Butler A, Dean DH. 2009. Proteomic analysis of the mosquito *Aedes aegypti*
905 midgut brush border membrane vesicles. J Insect Physiol 55:264-272.
906 59. Means JC, Passarelli AL. 2010. Viral fibroblast growth factor, matrix
907 metalloproteases, and caspases are associated with enhancing systemic infection by
908 baculoviruses. Proc Natl Acad Sci U S A 107:9825-9830.
909 60. Rojo G, Chamorro M, Salas ML, Vinuela E, Cuezva JM, Salas J. 1998. Migration of
910 mitochondria to viral assembly sites in African swine fever virus-infected cells. J
911 Virol 72:7583-7588.
912 61. Bandla MD, Campbell LR, Ullman DE, Sherwood JL. 1998. Interaction of tomato
913 spotted wilt tospovirus (TSWV) glycoproteins with a thrips midgut protein, a

potential cellular receptor for TSWV. Phytopathology 88:98-104.

62. Bautista RC, Mau RFL, Cho JJ, Custer DM. 1995. Potential of tomato spotted wilt tospovirus plant hosts in Hawaii as virus reservoirs for transmission by *Frankliniella occidentalis* (Thysanoptera: Thripidae). Phytopathology 85:953-958.

63. Martin K, Kopperud K, Chakrabarty R, Banerjee R, Brooks R, Goodin MM. 2009. Transient expression in *Nicotiana benthamiana* fluorescent marker lines provides enhanced definition of protein localization, movement and interactions in planta. Plant J 59:150-162.

64. Cilia M, Fish T, Yang X, McLaughlin M, Thannhauser TW, Gray S. 2009. A comparison of protein extraction methods suitable for gel-based proteomic studies of aphid proteins. J Biomol Tech 20:201-215.

65. Cilia M, Tamborindeguy C, Fish T, Howe K, Thannhauser TW, Gray S. 2011. Genetics coupled to quantitative intact proteomics links heritable aphid and endosymbiont protein expression to circulative polerovirus transmission. J Virol 85:2148-2166.

66. Dobson L, Remenyi I, Tusnady GE. 2015. CCTOP: a consensus constrained TOPology prediction web server. Nucleic Acids Res 43:W408-W412.

67. Nielsen H. 2017. Predicting secretory proteins with SignalP. Methods Mol Biol 1611:59-73.

68. Ioannidou ZS, Theodoropoulou MC, Papandreou NC, Willis JH, Hamodrakas SJ. 2014. CutProtFam-Pred: detection and classification of putative structural cuticular proteins from sequence alone, based on profile hidden Markov models. Insect Biochem Mol Biol 52:51-59.

69. Magkrioti CK, Spyropoulos IC, Iconomidou VA, Willis JH, Hamodrakas SJ. 2004. cuticleDB: a relational database of Arthropod cuticular proteins. BMC Bioinformatics

939 5:138.

940 70. Kumar S, Stecher G, Tamura K. 2016. MEGA7: molecular evolutionary genetics
941 analysis version 7.0 for bigger datasets. Mol Biol Evol 33:1870-1874.

942 71. Schwarz R, Dayhoff M. 1979. Matrices for detecting distant relationships, p 353-358.
943 *In* Dayhoff M (ed), Atlas of protein sequences doi:citeulike-article-id:2821320.
944 National Biomedical Research Foundation.

945 72. Jones DT, Taylor WR, Thornton JM. 1992. The rapid generation of mutation data
946 matrices from protein sequences. Comput Appl Biosci 8:275-282.

947 73. Adkins S, Choi TJ, Israel BA, Bandla MD, Richmond KE, Schultz KT, Sherwood JL,
948 German TL. 1996. Baculovirus expression and processing of tomato spotted wilted
949 tospovirus glycoproteins. Phytopathology 86:849-855.

950 74. Chakrabarty R, Banerjee R, Chung SM, Farman M, Citovsky V, Hogenhout SA,
951 Tzfira T, Goodin M. 2007. PSITE vectors for stable integration or transient
952 expression of autofluorescent protein fusions in plants: probing *Nicotiana*
953 *benthamiana*-virus interactions. Mol Plant Microbe Interact 20:740-750.

954

Table 1. Identification of *Frankliniella occidentalis* larval proteins bound to purified virions of *Tomato spotted wilt virus* in two-dimensional (2-D) gel overlays.

Spot Number	*Fo* Seq contig match[a]	Mascot score ($P < 0.05$)	Percent coverage[b]	Number of matched peptides	Peptide sequence(s)	Blastx annotation[c] ($E < 10^{-20}$)	Conserved motifs ($E < 10^{-10}$)
1	contig01248	279	37%	4	R.AQQPYQQYLQNQQFQNYQQR.A R.AAAAPILQYSNDVNPDGSFQYSYQTGDGISAQAAGFTR.N K.DAEAQVVQGSYSYTGPDGVVYTVNYIADENGYR.A K.ALPYYNQQQATYQQQQAAYQR.P	endocuticle structural glycoprotein	Chitin_bind_4
	CL4854Contig1	363	29%	7	R.VFFDMTVDGQPAGR.I R.ALCTGEQGFGYK.G R.VIPNFMCQGGDFTNHNGTGGK.S R.KFADENFQLK.H K.HTGPGIMSMANAGPNTNGSQFFITTVK.T K.TSWLDNKHVVFGSVIEGMDVVK.K K.HVVFGSVIEGMDVVK.K	cyclophilin	Cyclophilin_ABH
2	contig01248	77	10%	1	K.DAEAQVVQGSYSYTGPDGVVYTVNYIADENGYR.A	endocuticle structural glycoprotein	Chitin_bind_4
3	contig00018	196	25%	4	R.FGGALGGYNLAQTSQYHIQTDEGPER.Y R.LEDGTVVGTYGWVDADGYLR.L R.PYYPSSTPAVSLVSSTPR.P R.PYYPTSTPAVVSSTPR.P	uncharacterized, similar to cuticular protein	Chitin_bind_4
	contig14634	134	22%	3	R.GYISELPGTYDANSNSVIPEYDGIAVTHNGFR.Y K.AGSFGYVDPFGIR.R R.VIYYNTSPGSGFQVR.K	uncharacterized, similar to cuticular protein	none identified
	CL4900Contig1	113	10%	3	R.GYISELPGTYDASSNSVIPEYDGIAVTHNGFR.Y K.AGSFGYVDPFGIR.R R.VIYYNTSPGSGFQVR.K	uncharacterized, similar to cuticular protein	Chitin_bind_4
4	CL1591Contig1	76	5%	1	K.QESVYTAAQPAISTYK.K	flexible cuticular protein	Chitin_bind_4
5	CL1591Contig1	89	5%	1	K.QESVYTAAQPAISTYK.K	flexible cuticular protein	Chitin_bind_4
6	CL4854Contig1	615	30%	9	R.VFFDMTVDGQPAGR.I R.ALCTGEQGFGYK.G R.VIPNFMCQGGDFTNHNGTGGK.S R.KFADENFQLK.H	cyclophilin	Cyclophilin_ABH

					K.FADENFQLK.H K.FADENFQLKHTGPGIMSMANAGPNTNGSQFFITTVK.T K.HTGPGIMSMANAGPNTNGSQFFITTVK.T K.HVVFGSVIEGMDVVK.K K.KVVVADCGQLS		
7	CL4706Contig1	554	47%	17	R.GNPTVEVDLVTELGLFR.A R.AAVPSGASTGVHEALELR.D K.AIDNVNNIIAPELIK.S K.EIDELMLK.L K.LGANAILGVSLAVCK.A K.HIADLAGNTNIILPTPAFNVINGGSHAGNK.L K.LAMQEFMILPTGASSFK.E K.FGLDSTAVGDEGGFAPNILNNK.E K.EGLTLIIDAIAK.A K.VEIGMDVAASEFYK.D K.VEIGMDVAASEFYKDGQYDLDFK.N K.DGQYDLDFKNPNSDK.S K.LTDLYMEFIK.E K.EFPMVSIEDPFDQDHWDAWTTITGK.T K.TNIQIVGDDLTVTNPK.R K.VNQIGSVTESIQAHLLAK.K R.SGETEDTFIADLVVGLSTGQIK.T	enolase	Metal_binding
	contig12136	96	24%	2	R.QGDVVQGSYSLVEPDGSR.R R.TVEYTADPVNGFNAVVHK.D	cuticular protein	Chitin_bind_4
	contig14594	102	3%	1	R.TVDYTADPVNGFNAVVR.K	nuclear cap-binding protein	*RRM_NCPB2; Chitin_bind_4
	CL504Contig1	113	19%	2	K.AAVAVDTDYDPNPSYNYAYDIHDSLTGDAK.S R.TVEYTADPVNGFNAVVHK.E	cuticular protein	Chitin_bind_4
8	CL4706Contig1	407	43%	15	R.GNPTVEVDLVTELGLFR.A R.AAVPSGASTGVHEALELR.D K.AIDNVNNIIAPELIK.S K.HIADLAGNTNIILPTPAFNVINGGSHAGNK.L K.LAMQEFMILPTGASSFK.E K.FGLDSTAVGDEGGFAPNILNNK.E K.EGLTLIIDAIAK.A K.VEIGMDVAASEFYK.D K.VEIGMDVAASEFYKDGQYDLDFK.N K.DGQYDLDFKNPNSDK.S K.LTDLYMEFIK.E K.EFPMVSIEDPFDQDHWDAWTTITGK.T K.TNIQIVGDDLTVTNPK.R	enolase	Metal_binding

				K.VNQIGSVTESIQAHLLAK.K R.SGETEDTFIADLVVGLSTGQIK.T		
CL504Contig1	99	12%	1	K.AAVAVDTDYDPNPSYNYAYDIHDSLTGDAK.S	cuticular protein	Chitin_bind_4

[a]*de novo*-assembled contigs from *F. occidentalis* transcriptome derived by Roche 454/Sanger EST library hybrid (52)
[b]highest percent coverage obtained among the three picking gels used to collect protein spots for identification using ESI mass spectrometry
[c]NCBI Blastx search of the non-redundant protein database with the matching *Fo* nucleotide sequence contig query
*chimeric contig (= ambiguous annotation) - domains occur in opposite orientation on different ORFs

Table 2. Identification of *Frankliniella occidentalis* larval proteins bound to recombinant glycoprotein-N (G_N) in two-dimensional (2-D) gel overlays.

Spot Number	*Fo* Seq contig match[a]	Mascot score ($P < 0.05$)	Percent coverage[b]	Number of matched peptides	Peptide sequence(s)	Blastx annotation[c] ($E < 10^{-20}$)	Conserved motifs ($E < 10^{-10}$)
1	CL4310Contig1	595	27%	12	R.AAELSSILEER.I K.NIQADEMVEFSSGLK.G K.GMALNLEPDNVGIVVFGNDK.L K.GMALNLEPDNVGIVVFGNDKLIK.E R.TGAIVDVPVGDDLLGR.V K.TALAIDTIINQQR.F K.YTIIVAATASDAAPLQYLAPYSGCAMGEYFR.D K.HALIIYDDLSK.Q R.EAYPGDVFYLHSR.L R.EVAAFAQFGSDLDAATQQLLNR.G K.QGQYVPMAIEEQVAVIYCGVR.G K.IVTDFLASFNAASK	mitochondrial ATP synthase α subunit	AtpA
2	CL4310Contig1	302	12%	5	K.GMALNLEPDNVGIVVFGNDK.L R.TGAIVDVPVGDDLLGR.V R.VVDALGDAIDGK.G K.HALIIYDDLSK.Q K.IVTDFLASFNAASK	mitochondrial ATP synthase α subunit	AtpA
3	CL4382Contig1	633	43%	9	R.SSVVSQSVPVVSK.T K.SVPQYQQQYQTVSQYQSVPQYQQQVVVK.S K.SVPQYQQQVVVK.S K.SAPVYSQVHHVVEQQAAPVLLR.H R.TAFVPQYDSVSVSASAQPK.Y K.ILSQVQEFDPAGIYR.V R.VNFQTENGIQSAETGSVK.D R.ASGAHLPQVPEEIQR.S R.SLELNAAQPQKYDQDGNLVSQF	endocuticle structural glycoprotein	Chitin_bind_4
4	CL4382Contig1	137	15%	3	R.SSVVSQSVPVVSK.T K.SVPQYQQQYQTVSQYQSVPQYQQQVVVK.S R.VNFQTENGIQSAETGSVK.D	endocuticle structural glycoprotein	Chitin_bind_4
5	CL4382Contig1	169	22%	6	R.SSVVSQSVPVVSK.T K.SVPQYQQQVVVK.S R.VNFQTENGIQSAETGSVK.D R.ASGAHLPQVPEEIQR.S R.AAAEHGVAIVCPDTSPR.G K.ACQAVNMPVVLQMR.E	endocuticle structural glycoprotein	Chitin_bind_4
6	CL4382Contig1	1,154	53%	11	R.SSVVSQSVPVVSK.T K.SVPQYQQQYQTVSQYQSVPQYQQQVVVK.S	endocuticle	Chitin_bind_4

					K.SVPQYQQQVVVK.S K.SAPVYSQVHHVVEQQAAPVLLR.H R.HVEQEIPAYQSVQHVHQPVYQSVQHVAAHHVAAPVVSR.T R.TAFVPQYDSVSVSASAQPK.Y K.ILSQVQEFDPAGIYR.V R.VNFQTENGIQSAETGSVK.D R.VNFQTENGIQSAETGSVKDIQAK.D R.ASGAHLPQVPEEIQR.S R.SLELNAAQPQKYDQDGNLVSQF	structural glycoprotein	
7	CL4382Contig1	413	74%	8	R.SSVVSQSVPVVSK.T K.SVPQYQQQYQTVSQYQSVPQYQQQVVVK.S K.SVPQYQQQVVVK.S R.TAFVPQYDSVSVSASAQPK.Y R.VNFQTENGIQSAETGSVK.D R.VNFQTENGIQSAETGSVKDIQAK.D R.ASGAHLPQVPEEIQR.S R.SLELNAAQPQKYDQDGNLVSQF	endocuticle structural glycoprotein	Chitin_bind_4
8	CL4382Contig1	355	29%	7	R.SSVVSQSVPVVSK.T K.SVPQYQQQYQTVSQYQSVPQYQQQVVVK.S K.SVPQYQQQVVVK.S R.VNFQTENGIQSAETGSVK.D R.VNFQTENGIQSAETGSVKDIQAK.D R.ASGAHLPQVPEEIQR.S R.SLELNAAQPQKYDQDGNLVSQF	endocuticle structural glycoprotein	Chitin_bind_4
9	CL4382Contig1	155	5%	2	R.VNFQTENGIQSAETGSVK.D R.VNFQTENGIQSAETGSVKDIQAK.D	endocuticle structural glycoprotein	Chitin_bind_4
10	CL4382Contig1	130	4%	1	R.VNFQTENGIQSAETGSVK.D	endocuticle structural glycoprotein	Chitin_bind_4
11	CL4382Contig1	150	13%	7	R.SSVVSQSVPVVSK.T K.SVPQYQQQYQTVSQYQSVPQYQQQVVVK.S K.SVPQYQQQVVVK.SR.VNFQTENGIQSAETGSVK.D R.TAFVPQYDSVSVSASAQPK.Y R.VNFQTENGIQSAETGSVK.D R.VNFQTENGIQSAETGSVKDIQAK.D R.ASGAHLPQVPEEIQR.S	endocuticle structural glycoprotein	Chitin_bind_4

[a]*de novo*-assembled contigs from *F. occidentalis* transcriptome derived by Roche 454/Sanger EST library hybrid (52)
[b]highest percent coverage obtained among the three picking gels used to collect protein spots for identification using ESI mass spectrometry
[c]NCBI Blastx search of the non-redundant protein database with the matching *Fo* nucleotide sequence contig query

Table 3. Final candidate list of six TSWV-interacting proteins (TIPs)[a] from larval *Frankliniella occidentalis* to move forward to validation and biological characterization.

Putative protein	*Fo* Seq contig match[b]	ORF length[c] (nt/aa)	Signal peptide[d] (aa position)	Conserved domains[e]			Top Genbank match[f] (% coverage, % identity, *E*)
				Name	Position (aa)	E-value	
Cuticular protein-V (CP-V)	CL4900Contig1	1,302/434	1-18	Chitin_bind_4	447-92	$5.7x10^{-6}$	XP_017786818.1: PREDICTED: cell surface glycoprotein 1 [*Nicrophorus vespilloides*] (94%, 44%, $1x10^{-85}$)
Endocuticle structural glycoprotein-G_N (endoCP-G_N)	CL4382Contig1	852/283	1-15	Chitin_bind_4	190-246	$7.5x10^{-11}$	XP_018334183.1: endocuticle structural glycoprotein SgAbd-2-like [*Agrilus planipennis*] (33%, 53%, $4x10^{-22}$)
Endocuticle structural glycoprotein-V (endoCP-V)	contig01248	522/173	1-17	Chitin_bind_4	63-119	$1.4x10^{-18}$	XP_022906571.1: endocuticle structural glycoprotein SgAbd-2-like [Onthophagus taurus] (63%, 58%, $2x10^{-35}$)
Cyclophilin (peptidyl-prolyl cis-trans isomerase)	CL4854Contig1	618/205	None	cyclophilin_ABH_like PpiB Pro_isomerase	44-202 57-196 47-201	$2.3x10^{-120}$ $2.6x10^{-63}$ $1.2x10^{-62}$	XP_019753975.1: PREDICTED: peptidyl-prolyl cis-trans isomerase [*Dendroctonus ponderosae*] (99%, 75%, $2x10^{-109}$)
Enolase	CL4706Contig1	1,302/433	None	PLN00191 enolase Eno Enolase_C	3-433 5-417 6-431 143-433	0 0 0 0	XP_019767728.1: PREDICTED: enolase-like [*Dendroctonus ponderosae*] (99%, 87%, 0)
Mitochondrial ATP synthase α	CL4310Contig1	1,665/554	None	PRK09281 AtpA F1_ATPase_alpha ATP-synt_ab	45-551 45-553 135-416 190-413	0 0 0 $6.1x10^{-117}$	XP_023718907.1: ATP synthase subunit alpha, mitochondrial [*Cryptotermes secundus*] (99%, 89%, 0)

[a]sequences deposited into National Center for Biotechnology Information (NCBI) GenBank with the following accessions: CP-V (MH884758), endoCP-G_N (MH884757), endoCP-V (MH884756), cyclophilin (MH884760), enolase (MH884759), and mitochondrial ATP synthase α (MH884761).

[b]*de novo*-assembled contigs from *F. occidentalis* transcriptome derived by Roche 454/Sanger EST library hybrid (52)
[c]prediction by NCBI ORF Finder (https://www.ncbi.nlm.nih.gov/orffinder/)
[d]prediction by Signal P (http://www.cbs.dtu.dk/services/SignalP/)
[e]prediction by NCBI Batch Web CD Search Tool (https://www.ncbi.nlm.nih.gov/Structure/bwrpsb/bwrpsb.cgi) (CDSEARCH/cdd v3.16); E-value cut-off = 10^{-5}, only specific hits shown
[f]Blastp search of NCBI nr protein database against TIP ORF as of August 06, 2018; top match indicates highest alignment (max) score

Figure Legends

Fig 1. Overlay assay using purified virions and *F. occidentalis* first instar proteins resolved in two-dimensional gels.

Total proteins (150 µg) extracted from pooled healthy first instar larvae (0-17-hour old) of *F. occidentalis* were resolved by 2-D gel electrophoresis and transferred to nitrocellulose membranes. After blocking, membranes were incubated overnight with (A) blocking buffer (negative control) or (B) purified TSWV at 25 µg/mL, and then incubated with polyclonal rabbit anti-TSWV G_N antiserum. Only protein spots that consistently bound to purified TSWV in three (spots 1, 2, 4, 6, and 7) and four (spots 3, 5, and 8) biological replicates of the overlay assay were collected from three individual picking gels and subjected to ESI mass spectrometry for protein identification. Protein spots observed in the no-overlay-control membrane represent non-specific binding and were not collected for further analysis. Molecular mass (in kilodaltons) is shown on the Y axis and pI (as pH range) is shown on the X axis.

Fig 2. Overlay assay using recombinant G_N and *F. occidentalis* first instar proteins resolved in two-dimensional gels.

150 µg total proteins extracted from pooled healthy first instar larvae (0-17-hour old) of *F. occidentalis* were resolved by 2-D gel electrophoresis and transferred to nitrocellulose membranes. The membranes were incubated overnight with (A) blocking buffer (negative control) or (B) recombinant TSWV G_N (3.5 µg/mL). Using the polyclonal rabbit anti-TSWV G_N, protein spots that consistently bound to the recombinant TSWV G_N in two (spots 1 through 11) biological replicates of the overlay assay were collected from two individual picking gels and subjected to ESI mass spectrometry for protein identification. Protein spots

observed in the no-overlay-control membrane represent non-specific binding and were not collected for further analysis. Molecular mass (in kilodaltons) is shown on the Y axis and pI (as pH range) is shown on the X axis.

Fig. 3 Antisera specificity against each TSWV-interacting protein (TIP) (peptide) using dot blot analysis. Peptides that were used for producing its antibody were diluted to 100 µg/mL (for cyclophilin, enolase, endoCP-G_N, endoCP-V, and mATPase), and 2.5 mg/mL (for CP-V), and 2ul of each peptide were used for each test. PBS buffer and pre-immune serum (500,000 × dilution) were used as controls. All six diluted peptides and two controls were loaded onto six nitrocellulose membrane strips. Each strip was first incubated with one specific primary antibody (0.5 µg/mL, generated in mice), then incubated with goat anti-mouse-HRP (1:5,000 dilution). Each membrane strip was developed independently.

Fig 4. Immunolabeling of TSWV-interacting proteins (TIPs) within first instar larvae of *F. occidentalis*. The synchronized first instar larvae (0-17-hour old) were kept on 7% sucrose solution for 3 hours to clean their guts from plant tissues. These larvae were then dissected and immunolabeled using specific antibodies against each TIP as indicated. Thrips tissues incubated with pre-immune mouse serum are depicted here. Confocal microscopy detection of green fluorescence (Alexa Fluor 488) represents the localization of each TIP. TIPs were mainly localized at foregut (FG), midgut (MG), which includes epithelial cells and visceral muscle (VM), principle salivary glands (PSG), tubular salivary glands (TSG), and Malpighian tubules (MT). All scale bars are equal to 50 μm.

Fig 5. Confirmation of interactions between TSWV proteins and TSWV-interacting proteins (TIPs) using bimolecular fluorescence complementation (BiFC) in *Nicotiana benthamiana*. Plants transgenic for a nuclear marker fused to cyan fluorescent protein (CFP-H2B) were infiltrated with suspensions of *Agrobacterium tumefaciens* transformed with plasmids encoding the G_N protein (full length or soluble form, G_N-S) and TIPs proteins (EndoCP-G_N, CP-V, Cyclophilin, mATPase, Enolase, EndoCp-V) fused to either the amino or carboxy terminus of yellow fluorescent protein (YFP). The designation of Y indicates this is the n-terminal half of YFP and FP represents the c-terminal half of YFP. The Y or FP position in the name indicates all are carboxy terminal fusions to the protein of interest. The positive interactors are seen by fluorescence of YFP in images shown in the 'BiFC' column. The 'CFP-H2B' column is indicated to give cellular reference, and the overlay between the two is also shown. The final column is the nucleus enlarged to show detail of the interacting TIPs within the cellular context. The first row is a representative negative control with a TIP and glutathione S-transferase (all thrips and virus proteins were tested with the negative control to rule out non-specific interactions). All scale bars are equal to 20 μm.

Fig 6. Validation of TSWV-interacting proteins (TIPs) with G_N, and identification of the interacting domain of endoCP-G_N using split-ubiquitin membrane-based yeast two hybrid (MbY2H). (A) Interactions between G_N and six TIPs. G_N was expressed as G_N-Cub, and TIPs were expressed as NubG-TIPs using MbY2H vectors. (B) Interactions between TSWV G_N and different regions of endoCP-G_N. EndoCP-G_N was expressed as either the N-terminal domain (amino acids 1-176 and 1-189) that includes the non-conserved region or the C-terminal region (amino acids 177-284 and 190-284) that includes the conserved Chitin_bind_4 motif (CHB4) of endoCP-G_N. Interactions between G_N-Cub and NubI, G_N-Cub and NubG were used as positive and negative controls respectively for all MbY2H assays. Co-transformation of pTSU2-APP and pNubG-Fe65 into NYM51 was used as another positive control (data not shown); DDO = yeast double dropout (SD/-Leu/-Trp) media, and QDO = yeast quadruple dropout (SD/-Ade/-His/-Leu/-Trp) media.

Figure 7. Co-localization of TSWV G_N and endoCP-G_N or cyclophilin in insect cells. Open reading frames of cyclophilin, endoCP-G_N, and TSWV G_N were cloned into *Drosophila* gateway vectors (with Hsp70 promotor and gateway cloning cassette), and the pHWR and pHWG expression plasmids were used for the following fusion proteins: cyclophilin-RFP, endoCP-G_N-RFP and TSWV G_N-GFP. The recombinant plasmids, pHWR-cyclophilin, pHWR-endoCP-G_N and pHWG-TSWV G_N were single or co-transfected into insect Sf9 cells. All transfection reactions were performed using Cellfectin II Reagent. The mock, no DNA treatment (top left panels) and co-transfection of pHRW and pHGW expression plasmids (bottom left panels) were used as controls. Cells were stained with DAPI 72- hours post-transfection, and then visualized using the Cytation 5 Cell Imaging Multi-Mode Reader (BioTek, Winooski, VT) to detect red and green fluorescence. The exposure

89 settings (LED intensity/integration time/camera gain) of the mock were set up as the baseline
90 parameters for image analysis, and treatments were set no more than the mock settings. Cells
91 were visualized with the 40x objective, and each scale bar represents 10 μm.

92 **Supporting Information**

93 **Fig. S1 Phylogenetic analysis of cuticle protein (CP) R&R consensus sequences in first**
94 **instar larvae of *F. occidentalis*.** The Neighbor-Joining (NJ) method was performed with the
95 Jones Taylor Thorton (JTT) matrix-based method for amino acid substitutions with Gamma
96 distribution to model the variation among sites. The bootstrap consensus tree (500 replicates)
97 was generated by the NJ algorithm with pairwise deletion for handling gaps. Branches
98 corresponding to partitions reproduced in less than 70% bootstrap replicates were collapsed.
99 The numbers shown next to branches indicate the percentage of replicate trees in which the
100 associated taxa (sequences) clustered together in the bootstrap test. The analysis involved 46
101 sequences – the three cuticular TSWV-interacting proteins (TIPs: cuticle protein-V (CP-V),
102 endocuticle structural glycoprotein-V (endoCP-V) and endocuticle structural glycoprotein-G_N
103 (endoCP-G_N) (blue text), the 'gold-standard' Pfam database extended R&R consensus
104 sequence (pf00379), 19 insect orthologous sequences obtained from NCBI GenBank, and 23
105 structural CPs and endoCPs (translated transcripts, designated with FOCC or CUFF
106 identifiers) previously reported to be differentially-expressed in whole bodies of TSWV-
107 infected L1s of *F. occidentalis* (27). There were 95 amino-acid positions in the final dataset.
108 RR1 and RR2 = Cuticle Protein Rebers and Riddiford (CPR family, RR1 and RR2 types)
109 extended consensus, a conserved chitin-binding motif (chitin_bind_4 = CHB4).
110
111 **Fig. S2 Individual channels of immune-labeled TSWV-interacting proteins (TIPs)**
112 **within first instar larvae of *F. occidentalis*.** The synchronized first instar larvae (0-17-hour
113 old) were dissected and immunolabeled using specific antibodies against each TIP as
114 indicated. Thrips tissues incubated with pre-immune mouse antiserum as controls are
115 depicted here. Confocal microscopy detected green fluorescence (Alexa Fluor 488) that
116 represents the localization of each TIP, red represents Alexa Fluor 594 labeled actin; blue

represents DAPI labeled nuclei. All scale bars are equal to 50 μM.

Fig. S3 Localization of TSWV-interacting proteins (TIPs) fused to green fluorescent protein (GFP) in *Nicotiana benthamiana*. Plants transgenic for an RFP-ER marker were infiltrated with *Agrobacterium tumefaciens* strain LBA 4404 suspensions of TIPs constructs. Each row indicates the specific TIP-GFP fusion in relation to the RFP-ER marker. The columns are as follows: GFP channel, RFP channel and the overlay between the two channels. All scale bars are equal to 20 μm.

Fig. S4. Co-expression of fusion proteins in Sf9 insect cells. Three control sets of recombinant plasmids were co-transfected into insect Sf9 cells to ensure that unfused autofluorescent proteins do not alter protein localization (cyclophilin, endo-CP-G_N, and G_N), pHWR-cyclophilin and pHGW (expression of cyclophilin-RFP and GFP); pHWR-endoCP-G_N and pHGW (expression of endoCP-G_N-RFP and GFP); pHRW and pHWG-TSWV G_N (expression of RFP and TSWV G_N-GFP). All transfection reactions were performed using Cellfectin II Reagent, and cells were stained with DAPI at 72 hours post transfection. The red and green fluorescence were detected by Cytation 5 Cell Imaging Multi-Mode Reader. The exposure settings (LED intensity/integration time/camera gain) of mock were set up as the baseline, and different treatments were set no more than the mock settings. Each scale bar represents 10 μm.

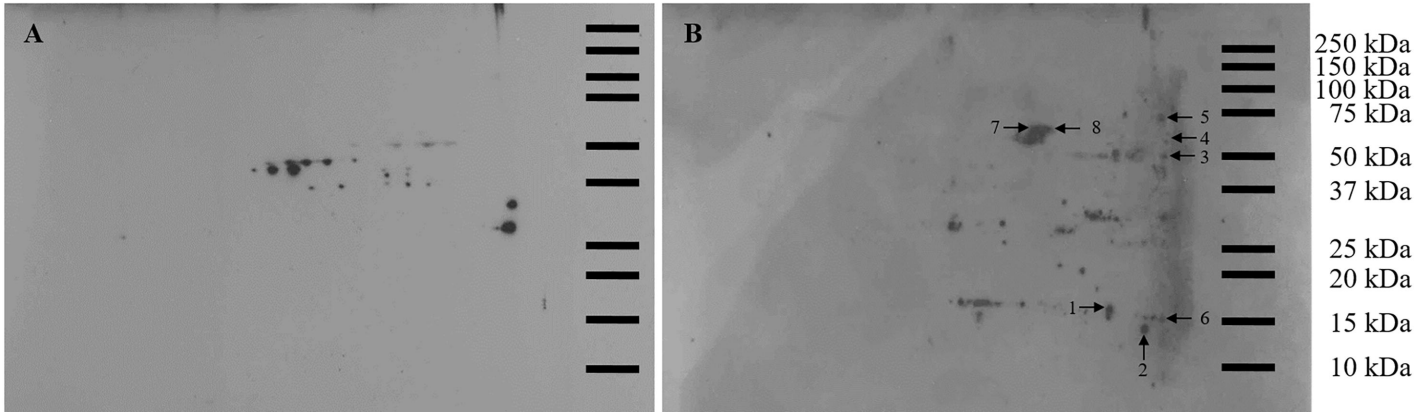
10
pH
3
A
10
pH
3
B
250 kDa
150 kDa
100 kDa
75 kDa
50 kDa
37 kDa
25 kDa
20 kDa
15 kDa
10 kDa
1
2
3
4
5
6
7
8

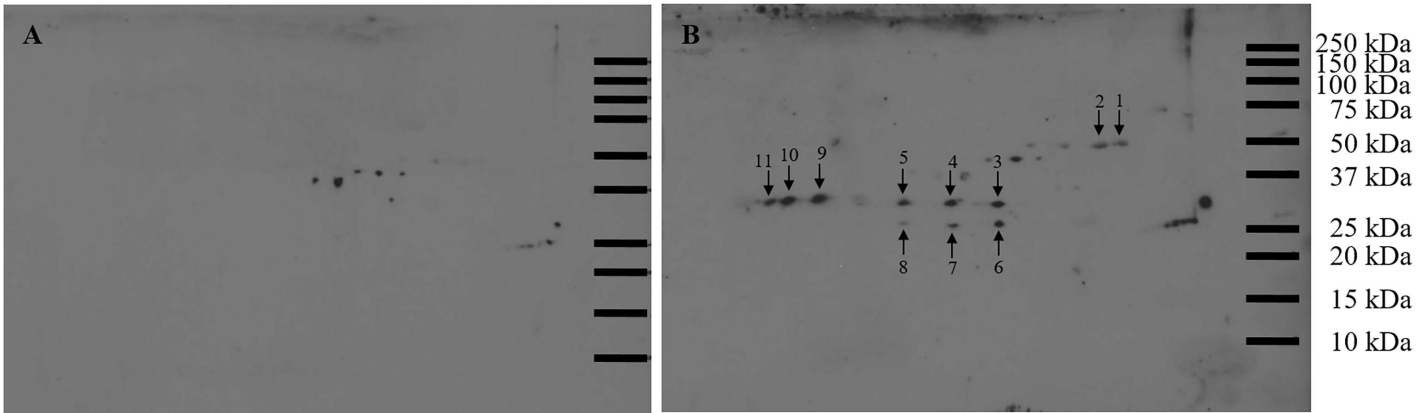
10
pH
3
A
10
pH
3
B
250 kDa
150 kDa
100 kDa
75 kDa
50 kDa
37 kDa
25 kDa
20 kDa
15 kDa
10 kDa
11
10
9
5
4
3
2
1
8
7
6

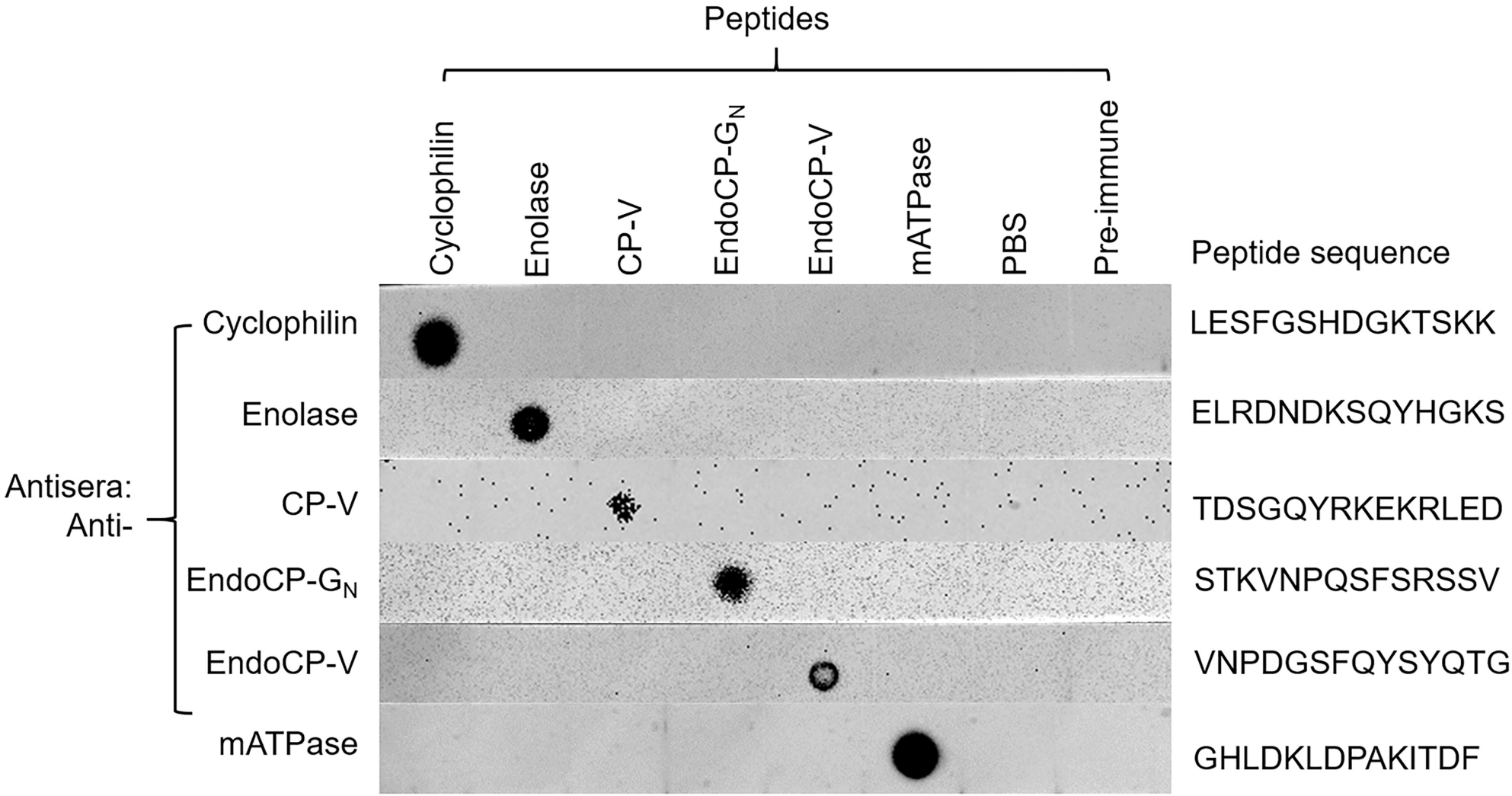
Peptides
Cyclophilin
Enolase
CP-V
EndoCP-G$_N$
EndoCP-V
mATPase
PBS
Pre-immune
Peptide sequence
Antisera:
Anti-
Cyclophilin
Enolase
CP-V
EndoCP-G$_N$
EndoCP-V
mATPase
LESFGSHDGKTSKK
ELRDNDKSQYHGKS
TDSGQYRKEKRLED
STKVNPQSFSRSSV
VNPDGSFQYSYQTG
GHLDKLDPAKITDF

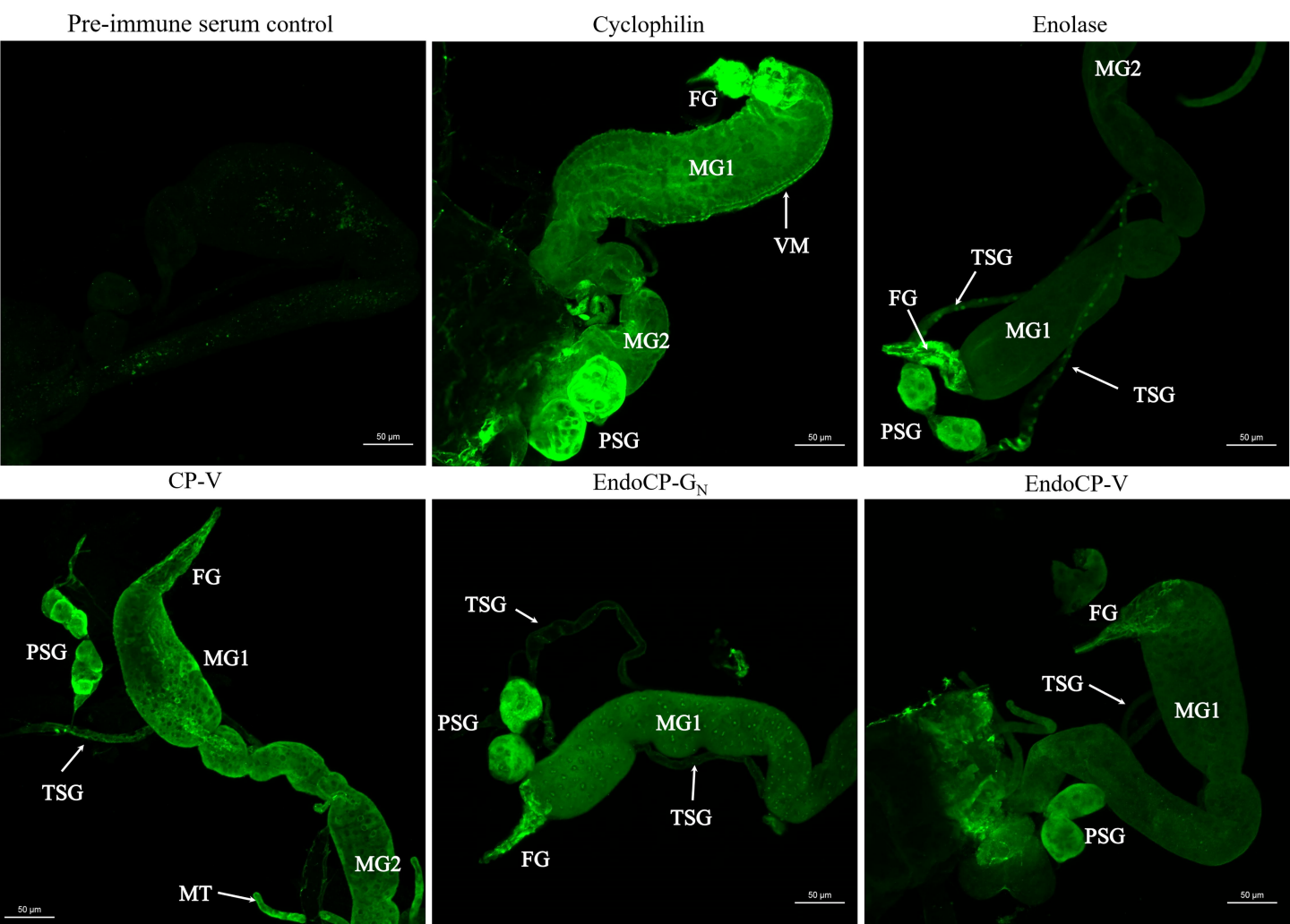
Pre-immune serum control
Cyclophilin
Enolase
FG
MG1
VM
MG2
PSG
TSG
FG
MG1
TSG
PSG
MG2
50 µm
CP-V
EndoCP-G$_N$
EndoCP-V
FG
PSG
MG1
TSG
MT
MG2
TSG
PSG
MG1
TSG
FG
FG
TSG
MG1
PSG

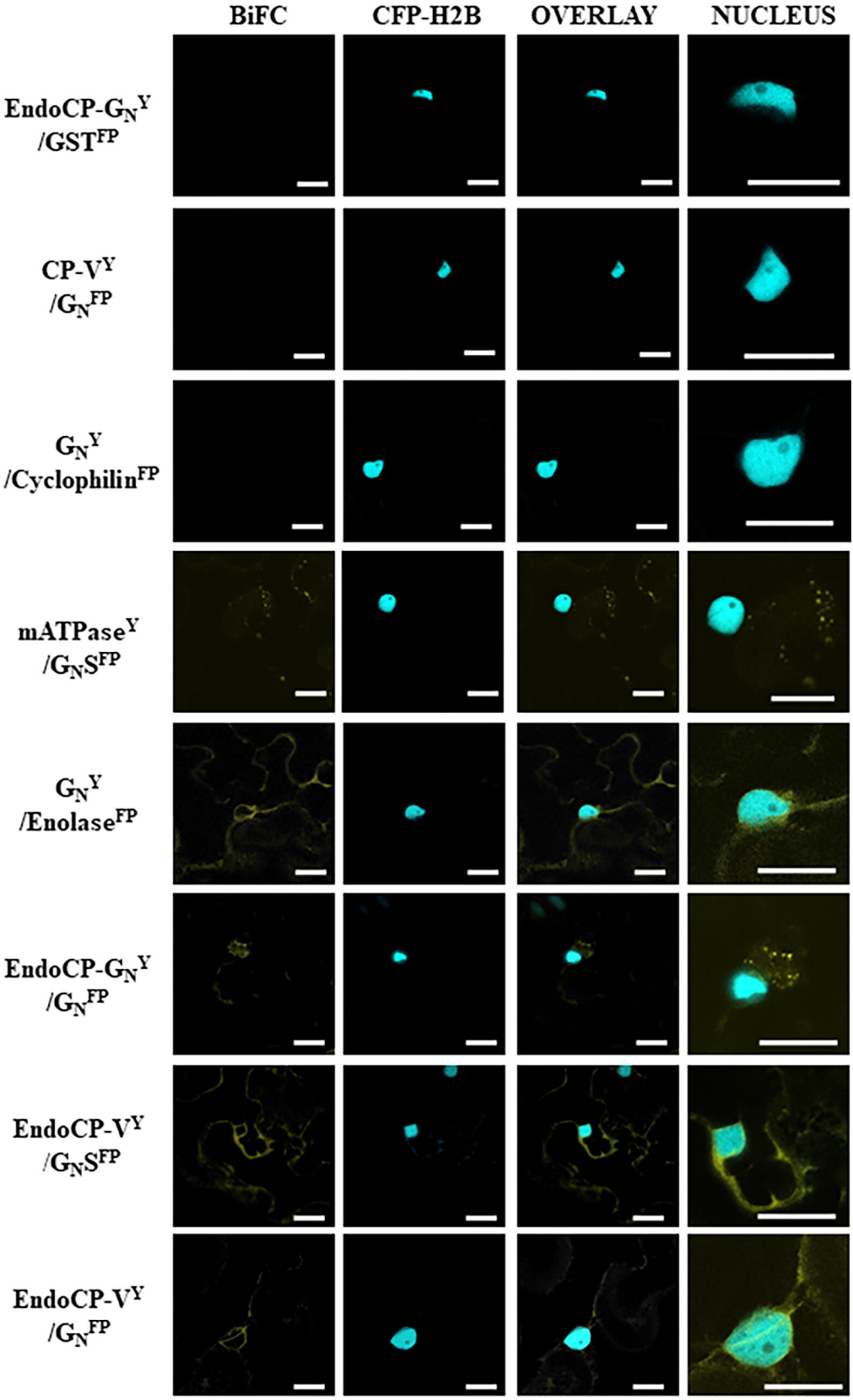
BiFC
CFP-H2B
OVERLAY
NUCLEUS
EndoCP-G$_N^Y$ /GST^{FP}
CP-V^Y /G$_N^{FP}$
G$_N^Y$ /Cyclophilin^{FP}
mATPase^Y /G$_N$S^{FP}
G$_N^Y$ /Enolase^{FP}
EndoCP-G$_N^Y$ /G$_N^{FP}$
EndoCP-V^Y /G$_N$S^{FP}
EndoCP-V^Y /G$_N^{FP}$

A

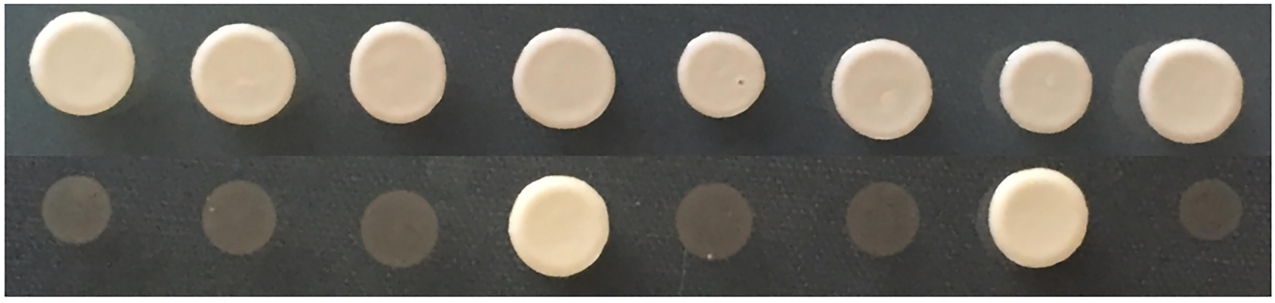
Cyclophilin + G_N
Enolase + G_N
CP-V + G_N
EndoCP-G_N + G_N
EndoCP-V + G_N
mATPase + G_N
NubI + G_N
NubG + G_N
DDO
QDO

B

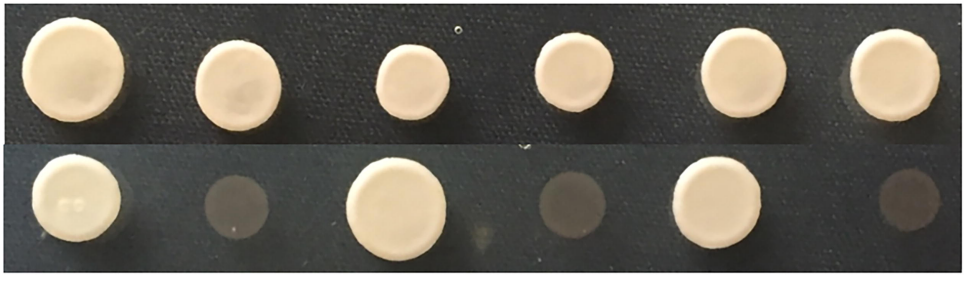
EndoCP-G_N 1-176 + G_N
EndoCP-G_N 177-284 + G_N
EndoCP-G_N 1-189 + G_N
EndoCP-G_N 190-284 + G_N
NubI + G_N
NubG + G_N
DDO
QDO

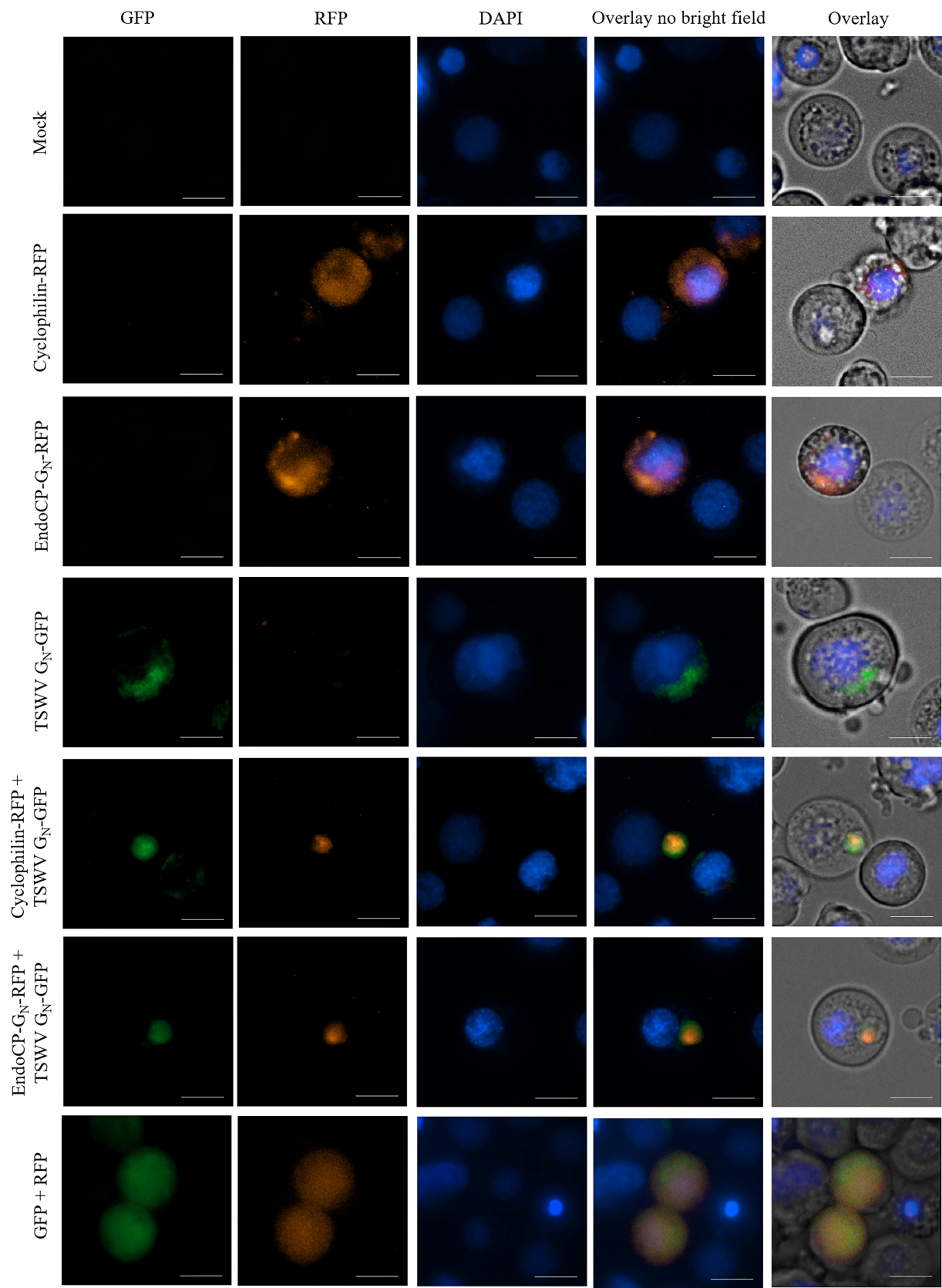
GFP
RFP
DAPI
Overlay no bright field
Overlay
Mock
Cyclophilin-RFP
EndoCP-G$_N$-RFP
TSWV G$_N$-GFP
Cyclophilin-RFP + TSWV G$_N$-GFP
EndoCP-G$_N$-RFP + TSWV G$_N$-GFP
GFP + RFP